Chapter 4

Title: **"High-Resolution, Large-Area, Nano Imprint Lithography"**

Principal Investigator:

Prof. Ki-bum Kim, Department of Materials Science and Engineering, Seoul National University, Korea

Telephone: +82-2-880-7095

Facsimile: +82-2-885-5820

E-mail: kibum@snu.ac.kr

Contract Number: FA4869-01-4048

AOARD Reference Number: AOARD-084048

AOARD **Program Manager:** Lt Col John Seo

Period of Performance: 2 year

Submission Date: 27 Aug 2009

Report Documentation Page

Form Approved
OMB No. 0704-0188

1. REPORT DATE	2. REPORT TYPE	3. DATES COVERED
27 AUG 2009	**FInal**	**01-05-2008 to 01-04-2009**

4. TITLE AND SUBTITLE
Chapter 1-4 Fundamental Nanoscience for Development of Devices II

5a. CONTRACT NUMBER
FA48690814048

5b. GRANT NUMBER

5c. PROGRAM ELEMENT NUMBER

6. AUTHOR(S)
Moonho Jo; Sooyoung Park; Younghee Lee; Kimbum Kim

5d. PROJECT NUMBER

5e. TASK NUMBER

5f. WORK UNIT NUMBER

7. PERFORMING ORGANIZATION NAME(S) AND ADDRESS(ES)
Korea Foundation for International Cooperation of Science & ,Technology (KICOS),275-7 Yangjae Dong, Seocho Gu,Seoul Korea (South),KR,275-7

8. PERFORMING ORGANIZATION REPORT NUMBER
N/A

9. SPONSORING/MONITORING AGENCY NAME(S) AND ADDRESS(ES)
AOARD, UNIT 45002, APO, AP, 96337-5002

10. SPONSOR/MONITOR'S ACRONYM(S)
AOARD

11. SPONSOR/MONITOR'S REPORT NUMBER(S)
AOARD-084048

12. DISTRIBUTION/AVAILABILITY STATEMENT
Approved for public release; distribution unlimited

13. SUPPLEMENTARY NOTES
This document contains results from four different basic research projects under the Phase I of US-Korea NBIT Program (2007-2010). It is the 2nd year results covering research results from 2008-2009.

14. ABSTRACT
Chapter 1 ? SiGe Alloy Nanowire Photonics; Chapter 2 ? Self-Assembled Liquid Crystalline Gels: From Nanostructure to Function; Chapter 3 ? Extremely Low Noise CNT for Peltier and Photo-dector Device Application; Chapter 4 ? High-Res, Large-Area, Nano Imprint Lithography;

15. SUBJECT TERMS
Nanotechnology of Liquid Crystal, nanolithography, nanodevices, Carbon nano tubes

16. SECURITY CLASSIFICATION OF:			17. LIMITATION OF ABSTRACT	18. NUMBER OF PAGES	19a. NAME OF RESPONSIBLE PERSON
a. REPORT	b. ABSTRACT	c. THIS PAGE			
unclassified	**unclassified**	**unclassified**	**Same as Report (SAR)**	**51**	

Progress Report

(USPI = Prof. Sungho Jin, UC San Diego, KPI = Prof. Ki-Bum Kim, Seoul National Univ.)

Project Title

HIGH-RESOLUTION, LARGE-AREA, NANO IMPRINT LITHOGRAPHY USING ELECTRON LATTICE IMAGES AND ELECTRON-EMITTING NANOPROBES

The development of large area nano imprint lithography techniques for applications such as ultra-high-density, patterned magnetic recording media with at least 1 terabit/in^2 recording density, about 5 times higher than the current hard disk memory in the market, is the major goal of this joint research project between SNU and UCSD. Such a high recording density requires a patterned media with the recorded magnetic island bit size of ~12.5 nm in diameter.

The fabrication of nano imprint stamp with high density and high aspect ratio is a key issue in the nano imprints lithography techniques. For the fabrication of nanopillar array pattern with sub-20 nm through atomic image projection electron beam lithography (AIPEL) and the conventional e-beam lithography, SNU introduce several techniques. – (1) fistly, the noise reduction process by Fourier filtering is introduced in AIPEL system to get rid of undesirable signals in mask signal. (2) The nano imprint is successfully performed using the NIL stamp with Si nano pillar array down to 25 nm pitch. (3) The SF_6+O_2 RIE is introduced to overcome the collapse of nanopillars sub-20nm pitch after the Cl_2 RIE. (Part I : Process development for the fabrication of nano impint stamp with sub-20nm pitch)

In addition to fabrication of nano-array patterned structure and imprint stamps that the SNU-UCSD joint R&D team is pursuing, there are some other major issues that need to be resolved for successful fabrication of viable, sub-20 nm magnetic recording media --- (1) One issue is the problem of magnetic switching field distribution (SFD) among various writable bits. (2) The second issue is the difficulty of read/write head (slider) flyability on patterned media disk due to the surface roufhness induced aerodynamic dragging. (3) The third issue, more relevant for FEPEL (Field Emission Projection E-beam Lithography) type nanofabrication is the difficulty of fabricating an extremely sharp tips on probe cantilevers. (4) The fourth issue is the difficulty of measuring the magnetic properties of small (sub-20 nm size) magnetic bit islands, especially for the laboratory samples with relatively small, patterned land of a few hundred micrometer size. (Part II : Issues on magnetic properties measurement in sub-20 nm size nano dot array)

Part I : Process development for the fabrication of nano imprint stamp with sub-20nm pitch

(1) Development of AIPEL process : introduction of noise reduction aperture.

We introduce the noise reduction aperture with 5 μm aperture size in AIPEL system in order to effectively remove the low frequency noise in the mask signal which is severely affect the quality of nano patterns such as uniformity. The NR aperture with 5 μm size is drilled in Mo thin foil with 10 μm thickness by focused ion beam machine. Figs. 1 show the HRTEM image without and with NR aperture [Fig. 1 (a) and (c)] and simulation results about NR aperture effect [Fig. 1 (b)]. The simulation and experimental results using NR aperture with 5 μm size is apparently same results. When the NR aperture with 5 μm size is applied, the low frequency noises which exist near the transmitted beam in the fast Fourier transform image (the insets of Fig. 1) is more effectively removed. Fig. 1 (d) ~ (f) shows the intensity profile extracted from the HRTEM image of Fig. 1 (a) ~ (c), respectively. The variation of maximum intensity is reduced after the NR aperture insertion. In experiment using NR aperture in AIPEL, the modulation transfer function (MTF) value is increased from 0.3 to 0.4 while the electron beam current is decreased to 50 %.

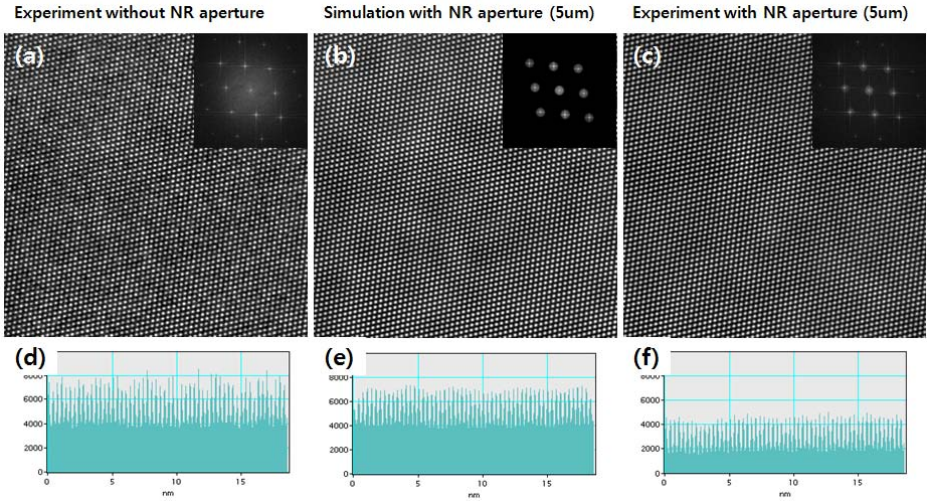

Fig. 1 Simulation and experimental results using noise reduction aperture. (a) and (d) experimentally obtained HRTEM images and its intensity profile, (b) and (e) simulation results on the 5 μm NR aperture, and (c) and (f) experimental results using NR aperture with 5 μm.

Fig. 2 shows the patterning results of Si nanopillar array using NR aperture. Fig. 1 (a) and (b) is a result at 200 (66 nm pitch) and 160 (53 nm pitch) magnification, respectively. At the 160 magnification, the dot size is about 26nm.

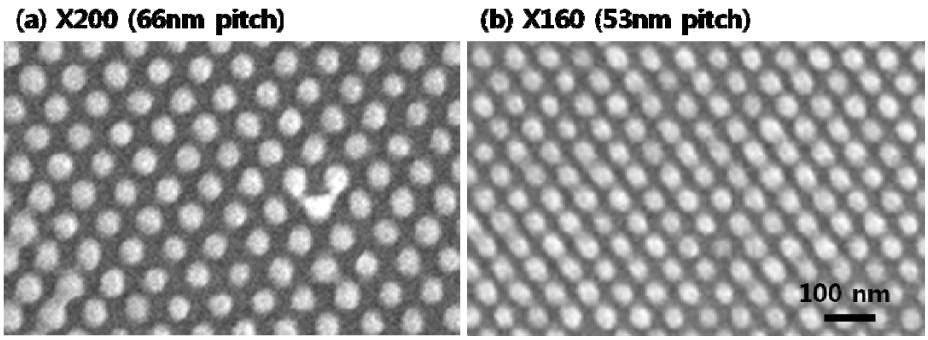

Fig. 2 Patterning results using NR aperture through AIPEL process. (a) 200 magnification (66 nm pitch) and (b) 160 magnification (53 nm pitch).

(2) Nano imprint results using stamp with 25 nm Si nano pillar array fabricated in 1st year.

The Si nano pillar array with 1 terabit/in^2 using conventional electron-beam lithography with 100kV is also developed. In the e-beam lithography, HSQ is selected as a resist which is known as one of the high-resolution e-beam resists with a patterning capability of less than 10 nm in a low density dot and line patterns. However, the minimum feature size with a high density pattern is still close to or larger than 20 nm. Processing steps for the formation of Si nano-pillar array is composed by e-beam lithography, Si etching by Cl_2 plasma, and strip of remained resist. With the conventional processing scheme, we can successfully fabricate Si nano-pillar array with the pitch size larger than 30 nm as shown in Fig. 3(a) ~ 3 (c). However, resist patterns below the 25 nm pitch were not isolated and merged each other due to the e-beam proximity effect. This effect certainly limits the patterning capability which is less than 25 nm. Here, we propose a novel development process of HSQ resist using diluted HF solution in between the conventional TMAH development process, which is called to "two-step development". (The detail fabrication process of Si nano pillar array is explained below this page[1].) Using this method, we can obtain fully isolated resist pattern with pitches

[1] Hydrogen silsesquioxane (HSQ) dissolved in methyl isobutyl ketone (MIBK) was spin-coated on the Si substrate with a thickness of 30 nm and baked at 90 ^oC on a hot plate for 1 min. The HSQ solution (Fox-12) was purchased from Dow Corning. The e-beam exposure was carried out using AIPEL system with 200 keV and a JEOL JBX9300FS with a beam radius of about 2 nm at the accelerating voltage of 100 keV. Dot array patterns of various pitches from 15 nm to 50 nm were exposed with e-beam dose of 1.0 ~ 3.0 mC cm^{-2}. Development was carried out in tetramethylammonium hydroxide (TMAH) 25 % aqueous solution at 21 ^oC for 1 min, followed by rinsing with H_2O for 2 min. Two step development process follows three steps: the first dipping in TMAH solution, the siloxane layer removal step using a dilute hydrofluoric acid (HF) solution (4000:1 DI water:HF), and the second dipping in TMAH solution. The patterned HSQ and Si substrate were etched for 1 min by Cl_2 plasma (operating pressure; 10 mTorr, plasma power; 75 W) using an RF plasma chamber (Oxford plasmalab 80). After dry etching step, residual HSQ was removed by HF dip.

Formatted: Font: 10 pt

from 25 nm down to 15 nm, and the resist pattern with 25 nm pitch was well transferred to the Si substrate [Fig. 3 (d)]. The mean diameter and height of them are 20 and 45 nm, respectively. The nano imprint stamp with Si nanopillar array with 25 nm pitch is successfully fabricated and the nano imprint lithography is performed using this stamp. Fig. 4 shows the SEM micrographs of nano imprint results with various pitches from 50 nm to 25 nm. These results was published in "SMALL" in 2008.

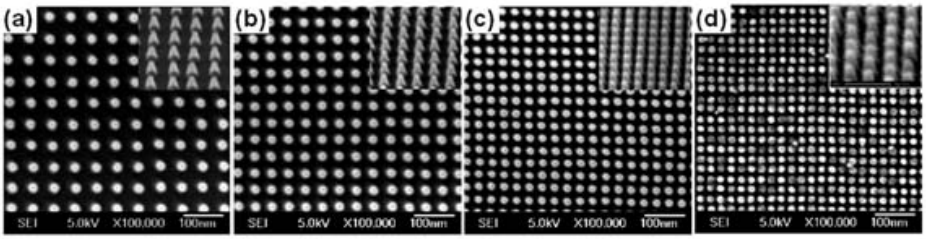

Fig. 3 Plan-view SEM images of the Si nano-pillar array with pitches of (a) 50 nm, (b) 40 nm, (c) 30 nm and (d) 25 nm. The insets are the SEM images tilted view.

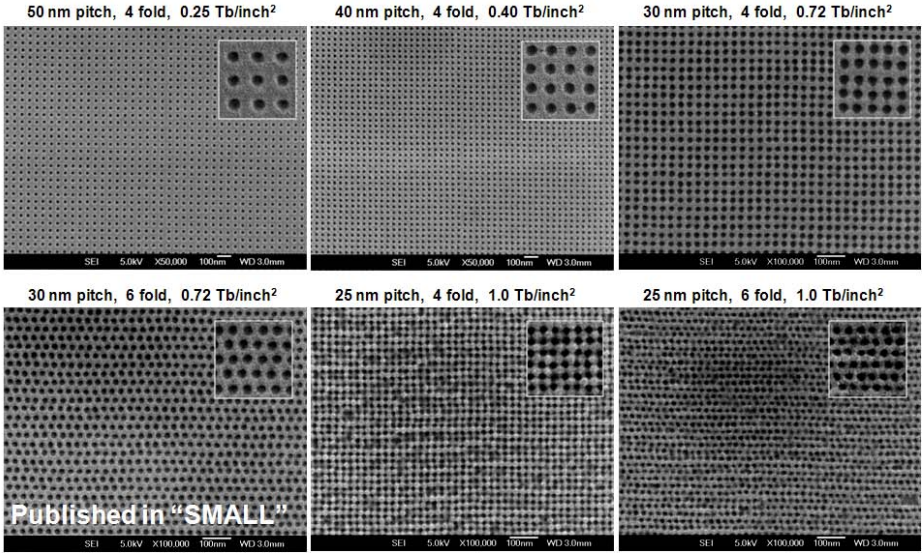

Fig. 4. Nano imprint results using the stamp with Si nano pillar array

(3) Process development for the fabrication of NIL stamp with sub-20 nm feature : introduction of SF_6+O_2 RIE

It is also noted that the resist patterns of 20 and 15 nm pitches were not successfully transferred to Si substrate which is shown in Fig. 5. We believe that this is due to the limitation of plasma etching (anisotropy characteristic of plasma etching), which generates the sidewall profile of etched pattern. Fig. 6 show the Si nano-pillar morphology after Cl_2 RIE process. Nano-dot pattern (HSQ resist) diameter with 15nm is increased to 20 nm after 30nm thickness etching by Cl_2 RIE, which may be due to the isotropic etching by Cl_2. Thus, the nano-dot has a side slope of 84^o which is confirmed by tilted view SEM micrograph. If the dot-to-dot pitch is decreased below 25 nm, the 20nm dots are merged and disappeared by Cl_2 RIE which schematics shows in Fig. 6. Moreover, we cannot make the Si nano pillar array with high aspect ratio over 1:1.

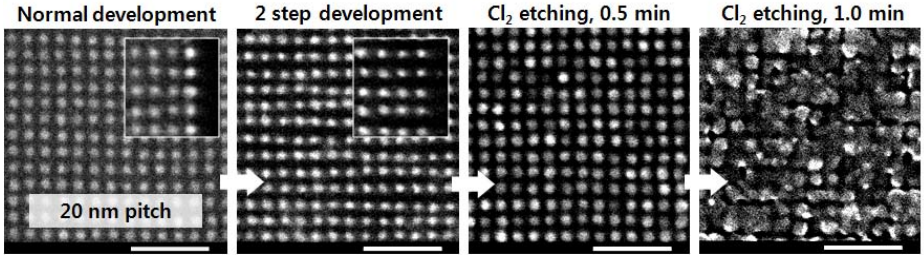

Fig. 5 Limitation of sub 20 nm pattern transfer using Cl_2 RIE

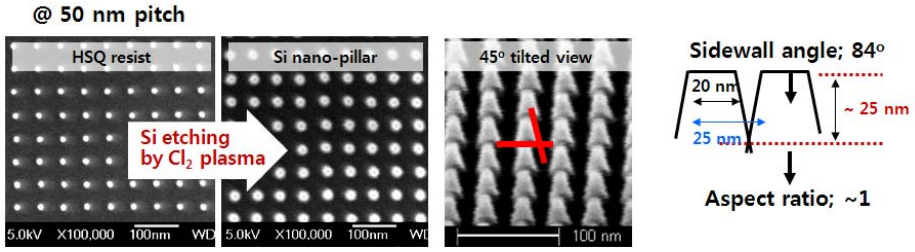

Fig. 6 The profile of Si nanopillar array using Cl_2 RIE

Consequently, we introduce the SF_6 RIE etching process with high selectivity between Si and HSQ in order to prevent the positive side wall slop of nano-pillars after RIE. While etching selectivity of Cl_2 RIE is about 3, the etching selectivity of SF_6 is about 5. (See Fig. 7) After SF_6 RIE, Si nano-pillars fall down by undercut because SF_6 gases chemically etch the Si substrate. In order to prohibit the undercut, O_2 gas is introduced in etching species. Fig. 7 shows the etching rate and etching selectivity between Si and HSQ as a function of O_2 ratio. Etching rate of Si by SF_6+O_2 RIE is decreased from 120 nm/min to 50 nm/min with increasing the O_2 ratio, while etching rate of HSQ keeps a similar value of ~ 30 nm/min. Because of the decrease of Si etching rate, the etching selectivity is decreased from 5 to 1 with increasing O_2 ratio from 1 % to 50 %. We set to the etching condition of 70% SF_6 + 30% O_2 gas mixture with high selectivity over 4 and perpendicular side wall profile of nano-pillar. Fig. 8 show the Si nano-pillar

morphology after SF_6+O_2 RIE. After RIE, the increase of dot size is not observed and nano-pillars have a side wall of ~90^o which is shown in Fig. 8 (right figurea)

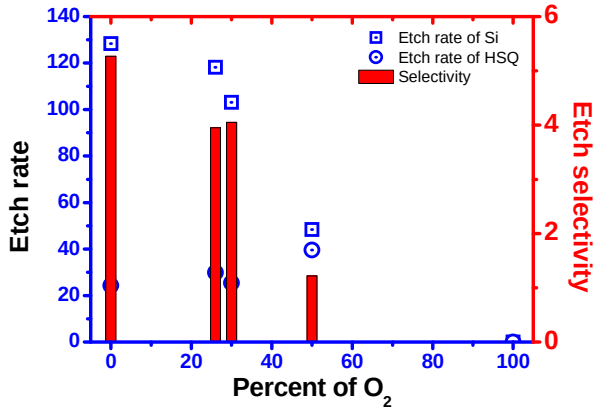

Fig. 7 etch rate of Si and HSQ and etch selectivity as a function of O_2 ratio in SF_6 + O_2 gas mixture.

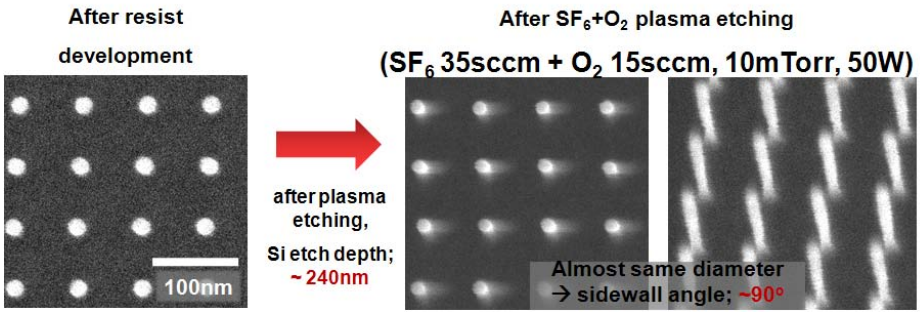

Fig. 8 The profile of Si nanopillar array using SF_6 + O_2 RIE

Part II : Issues on magnetic properties measurement in sub-20 nm size nano dot array

(1) **Magnetic switching field distribution**

In the technical field of patterned magnetic media (also called "Bit Patterned Media"), one of the current issues is the problem of magnetic switching field distribution (SFD). To operate the magnetic hard disk drive memory, the recorded bits need to be switched between "1" vs "0" (which is typically obtained by changing of magnetization directions through north pole - south pole switching. The desired magnetic field for switching of recorded bits in future high-density hard disk drive is typically ~5 – 10 KOe. Recent literatures report a substantial undesirable variation of the magnetic switching field when the size of the magnetic nano islands is reduced to below ~ 50 nm.

The switching field distribution is sometimes more than 30% from the median coercive force value, which is unacceptable from the hard disk memory application point of view. Various possible causes were discussed --- dimensional variations after lithographic patterning, islands sizes variations, islands edge effects, local compositional variation of Co and Pd at interfaces, distribution of intrinsic magnetic anisotropy, grain orientation and sizes or grain boundary variations.

Understanding of why such a switching field variation occurs in nanoscale dimensions, and how to prevent such a phenomenon are of paramount issue that has to be resolved for developing the ultra-high-density magnetic recording media so that the switching of bit information is carried out in a reproducible manner. While some of the recent literature report that the distribution of intrinsic magnetic anisotropy might be the cause for the switching field variation, there are additional possibilities for the cause of the SFD (switching field distribution) that have not been addressed. One of these possibilities include the fact that the shape of nano-magnet islands fabricated by e-beam lithography is not always uniform. Depending on the shape of the substrate Si pillars (vertical, positively tapered, or negatively tapered) as illustrated in Fig. 1, there can be some sidewall deposition of magnetic recording media, which can contribute to the observed SFD.

As magnetic layer deposition on top of protruding pillars tends to have some corner and sidewall deposition, this may cause different magnetic properties and switching fields, and may cause SFD in the magnetic islands. To investigate if removal of such sidewall deposition reduces the SFD problem, we modified the RIE parameters to intentionally alter the shape of the sidewall in Si nanopillars and introduced negative tapered Si column geometry as illustrated in Fig. 1. The figure shows ~30-50 nm diameter Si islands having the three different sidewall configurations, fabricated by e-beam lithography utilizing various RIE conditions.

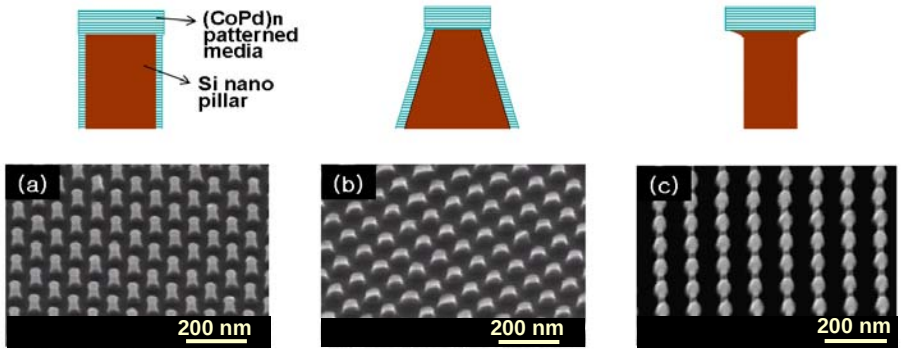

Fig. 1. Control of Si pillar sidewall configurations.

Based on reproducible Si nano-island array preparation, we have successfully fabricated patterned magnetic recording media as described in Fig. 2. About ~30 nm diameter Si pillar array was fabricated by E-beam lithography patterning as the basis to deposit magnetic material. High coercive force magnetic layer of multilayered magnet of (CoPd)n [n=8] with strong perpendicular magnetic anisotropy was deposited on the top surface of Si pillars. The structured multilayer nanomagnets consist of other adhesion layer and anisotropy-inducing layer by utilizing the geometry of Ta 3 nm\Pd 3 nm\[Co 0.3 nm\Pd 0.8 nm]$_8$. The coercivity was Hc ~4 KOe. (If FePt (L1o phase) is deposited, Hc of ~15KOe expected.)

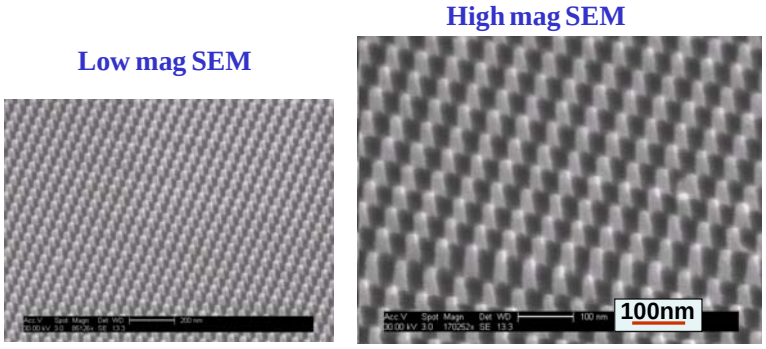

Fig. 2. Patterned magnetic recording media fabricated. The [CoPd]n islands with n=8 (~30 nm regime) were sputter deposited on Si nano pillars.

Comparative magnetic properties of patterned media islads with different sidewall configuration were evaluated using Micro MOKE measurements. As shown in Fig. 3 for the second quadrant M-H loop, the measurement data clearly indicates that the magnetic coercivity of [CoPd]n islands (~30 nm regime) on Si nano pillars with vertical sidewall has less variation in coercivity of ~15.3% in the switching field distribution (SFD) than that with positive side wall (~20.3%). Therefore it has been shown that the slanted geometry of the patterned media magnetic islands is less desirable than a vertical wall

geometry. The magnetic measurement for the negative slope geometry of Fig. 1(c) sample will be carried out to see if a further reduced SFD can be obtained.

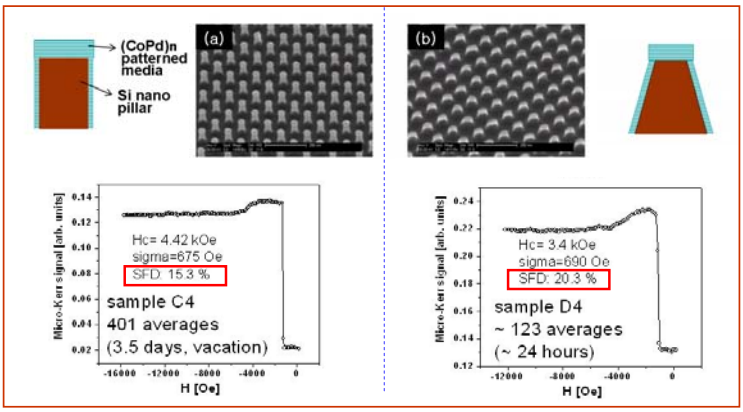

Fig. 3. Micro MOKE measurements of M-H loop for the patterned magnetic recording media, with the structured multilayer magnet of Ta 3 nm\Pd 3 nm\[Co 0.3 nm\Pd 0.8 nm]$_8$ sputter deposited on Si nano pillars.

(2) Read/Write head (slider) flyability on patterned media

When the magnetic material is deposited onto the lithographically pre-patterned substrate, the magnetic material in the trenches can introduce undesirable noise during Read/Write test, and also creates undesirable magnetic interactions between the magnetic materials deposited in the trench vs the island top. In order to minimize such deleterious effect, the height of the pillars must be tall enough. However, the read/write head can not smoothly fly over the patterned media if the depth of the trenches is too large, as we have observed with some of our island-patterned media as we attempted head flying experiments using standard Read/Write recording head for Co-Cr-Pt-SiO2 media. (For such a head flying experiments, randomly patterned nano-magnet structuresamples that we fabricated at UCSD with 5-50 nm diameter magnetic islands was used, since a large-area, hard disk size preparation was necessary, and since a disk-size periodic patterning with e-beam lithography would be too costly, e.g., many millions of dollars, at the moment).

To solve such a problem of recording head not being able to fly due to the drag of the trenches, we developed a technique of filling the trenches with a nonmagnetic material to planarize and make the hard disk surface as smooth as possible. We used the hydrogen silsesquioxane (HSQ) material to fill and planarize the trenches on a recording media disk because HSQ is easy to spin coating and the mechanical properties and thickness of the resultant SiO2 can be controlled for optimal read/write recording head flyability by changing the baking temperature after spin coating and plasma treatment. HSQ was spun over the patterned media to fill the grooves and re-etched slightly by reactive ion etch (RIE) to remove the overfilled part. As shown in Fig. 4, the SEM micrographs and AFM surface profiling data for trench depth measurements indicate that

the planarized patterned media exhibit a much smoother surface than the as-made patterned media surface.

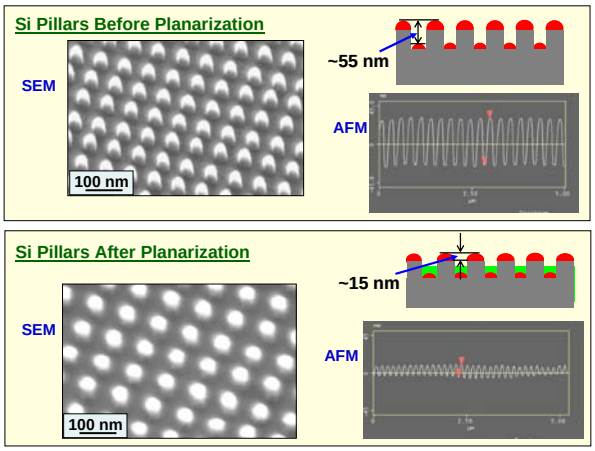

Fig. 4. (a) Comparative SEM microstructure of as-fabricated vs planarized nano-island patterned media using HSQ filling and back etching. (b) AFM profile of the patterned media sample surface before vs after planarization.

For some of the samples, intentional over-etch by RIE was used to artificially control the surface roughness (trench depth) for comparison purpose. The flyabilities of these planarized patterned media surface with various trench depths were measured and compared with that of the unplanarized patterned media as shown in Fig. 5. We used a slider which was designed to fly at a flying height of 11 nm at a velocity of 22 m/s. The slider didn't show any flyability on the as-patterned [Co-Pd]n disk with 40 nm bit height, while planarized disk allowed the head flying. Fig. 5(b) shows fluctuation of a slider on the planarized patterned media disk of which the depth of recess is ~0 nm. The fluctuation of a slider on this disk is almost the same as that of the unpatterned smooth media shown in Fig. 5(a). In this case, the standard deviation of flying fluctuation of a slider on the disk was 0.1 nm, while the standard deviation on the smooth disk was 0.09 nm. It shows very stable flying condition. As the final depth of recess is increased as 10 and 20 nm shown in Fig.5 (c) and Fig.5 (d), increased dragging interaction between the head and disk was observed. The standard deviation of flying fluctuation of a slider on those disks was 0.18 and 0.52, respectively. From this flyability test, we have demonstrated that the flaybility of a patterned media slider (read/write head) can be greatly improved with planarization.

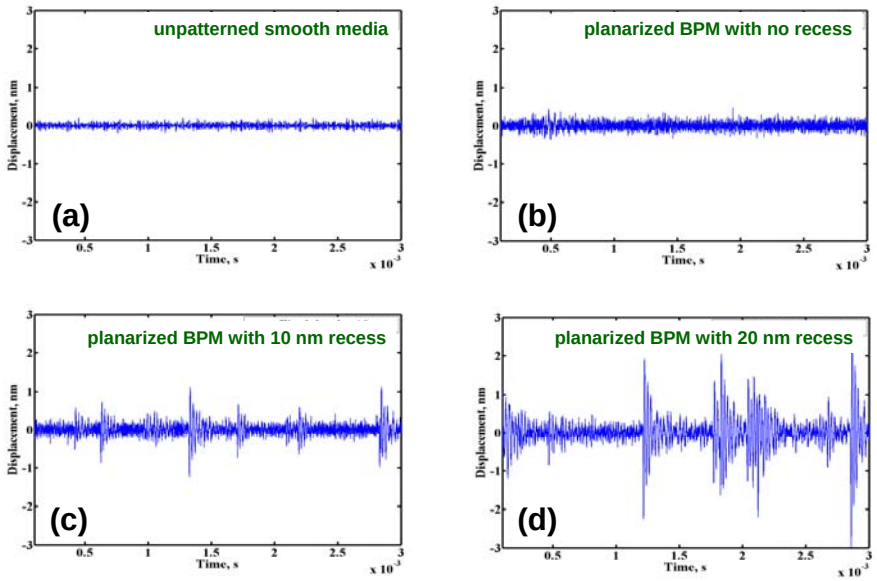

Fig. 5. Comparative measured fluctuation of flying read/write head slider, (a) unpatterned smooth media, (b) planarized patterned media with no recess, (c) planarized patterned media back etch to intentionally create an average 10nm recess, and (d) planarized patterned media with induced 20 nm recess.

(3) Fabricating extremely sharp tips on probe cantilevers

For FEPEL type lithography, extremely sharp field emitter tips, desirably less thatn 10 nm tip diameter, is desirable. Fabrication of such a tip on small cantilever is not always easy. We utilized electric-field-guided CVD growth of carbon nanotubes on Si cantilever to produce such a sharp tip. Shown in Fig. 6 is an example of tip geometry control by using the DC plasma electric field during the CVD growth to intentionally sputter and gradually reduce the CNT catalyst nanoparticles (Ni particles in this case) so that the nanotube diameter is also gradually reduced leading to extremely sharp tip configuration.

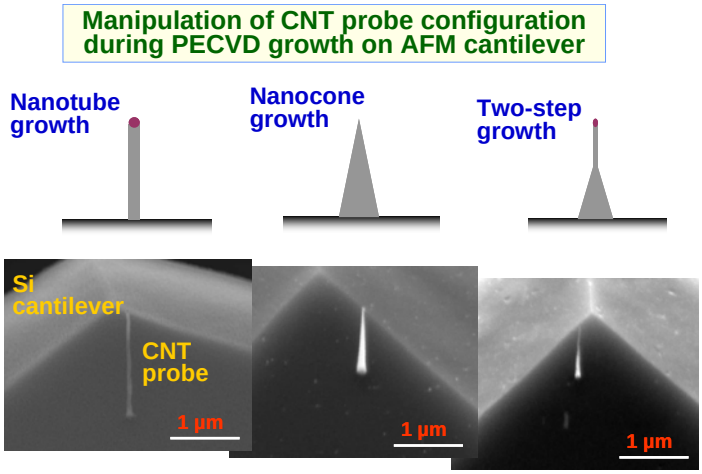

Fig. 6. Control of Carbon nanotube tip geometry on Si cantiler during CVD growth.

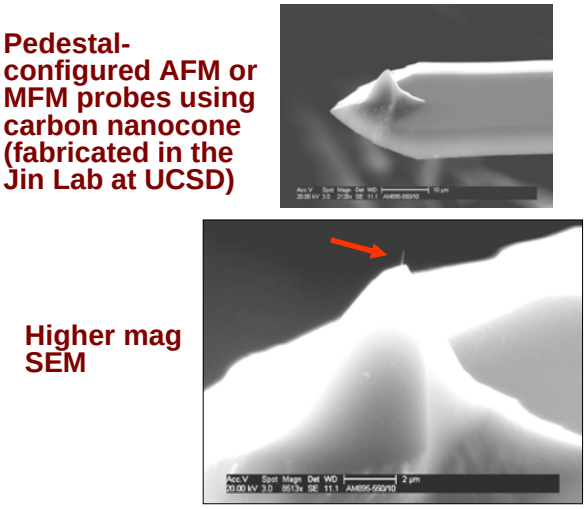

Fig. 7. SEM micrographs for the CNT probe made at UCSD, exhibiting sharp tip configuration grown on truncated AFM probe base.

An alternative material for field emitter tip is the silicon tip, which is easier to fabricate utilizing nanofab processes. We have prepared an array of extremely sharp Si tips (with just a few to several nanometer diameter tips) as shown in Fig. 8(a) – (c). A precursor nano-pillar array of Fig. 9, e.g., fabricated by nano-imprinting and RIE or chemical etching, can be used as the basis for such nanotip array fabrication. These silicon nanotip arrays can be fabricated easily by a combination of nano-imprinting and advanced RIE processing. To impart a lower-work-function, relatively easily field emitting tips, the surface of these tips will be either metallized by coating with a thin, stable metal (or alloy, or compound), or carburized to form a conductive or semiconductive carbide layer.

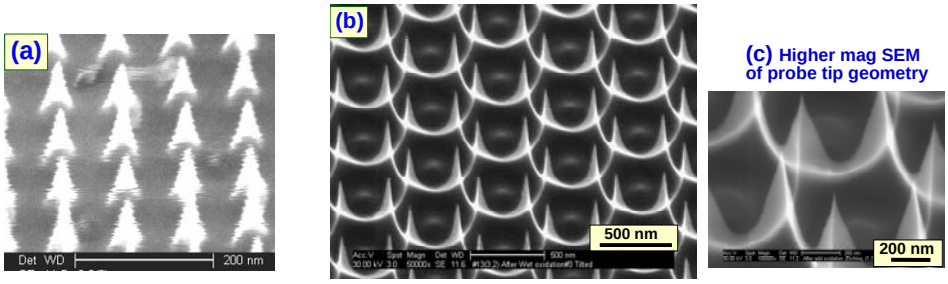

Fig. 8. SEM micrographs for Si nanotip array with very sharp tips for FEPEL probe arrays.

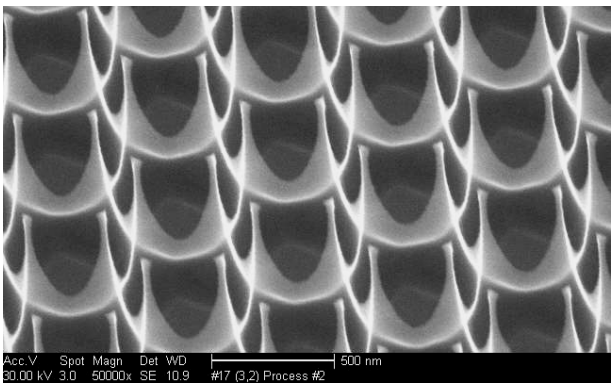

Fig. 9. SEM micrograph for Si pillar arrays in a large area (~0.5 x 0.5 cm area) containing a periodically arranged, ~35 nm diameter tips.

Shown in Fig. 10 is an array of ~10 nm diameter, periodic pillar array which can further be RIE etched to exhibit much sharper tip configuration.

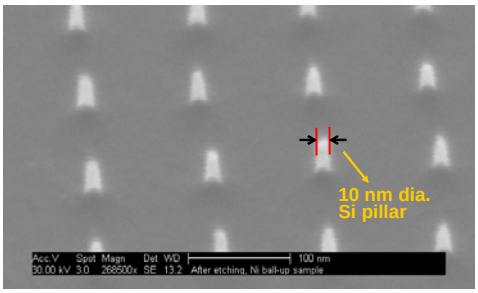

Fig. 10. Periodic ~10 nm dia. Si pillar array by E-beam lithography

(4) Sub-20 nm resolution MFM for Magnetic measurement of nanomagnets

For R&D progress of nanopatterning and preparation of nanomagnets, an evaluation of small area arrays of nanomagnets, such as typical e-beam lotho fabricated area of 10 x 10 or 100 x 100 μm samples is essential. However, the magnetic signals from such areas are very small, many orders of magnitude smaller than the typical resolution of SQUID machines.Therefore a development and optimization of MFM (magnetic force microscopy) probes for more accurate evaluation patterned media magnetic islands can be very useful. The patterned media magnetic materials, due to their small size, planar distribution and low volume fraction, are well beyond the available SQUID measurement resolution, and there is no other viable techniques except some home-made microMOKE (magneto Optical Kerr Effect) analysis apparatus available only in handful research institutes in the world. When the patterned media island size becomes ~10 nm regime, even the microMOKE will exhibit insufficient sensitivity to measure the M-H loop of these magnetic islands. Currently available MFM probe barely allow measurement of 40 nm magnetic islands.

Therefore, there is an urgent need to develop a new magnetic measurement technology. With the expertise at UC San Diego in fabricating ultra-sharp AFM probes using carbon nanotubes (see the SEM micrographs below), we are also planning to devote substantial amount of time and effort to develop new, ultra-sensitive magnetic measurement technology based on ~10 nm MFM probes and operational techniques. Such a new magnetic MFM probes will enable the study of magnetic switching properties by allowing M-H loop measurements on sub-20 nm island size patterned media, desirably to allow M-H loop characterization of individual islands.

Shown in Fig. 11 is the schematic illustration of a CNT cantilever tip for MFM tip application, made by sputter coating of high-coercivity Fe-Pt magnetic film. The CNT based MFM tips exhibits much enhanced resolution of Co-Cr-Pt-SiO2 recording media on MFM measurements.

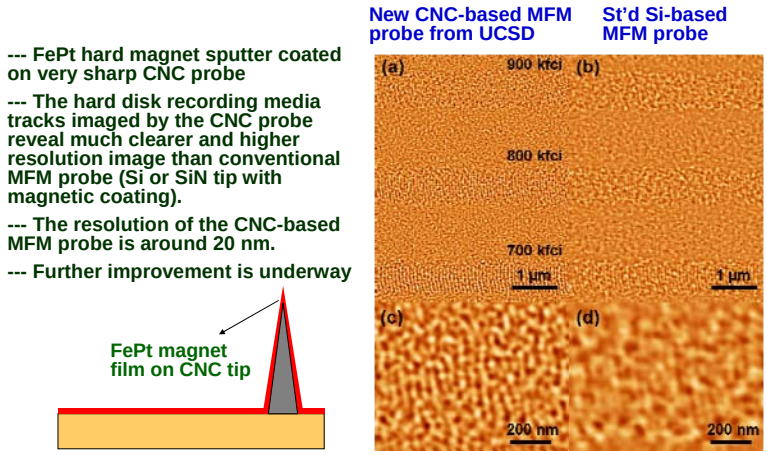

Fig. 11. FePt-coated Carbon Nanocone probes for improved MFM (magnetic force microscopy) imaging.

Currently a new MFM probes tips with sub 10 nm tips are being developed, Fig. 12, for eventual high-resolution MFM measurements of a single magnetic island. Here the high-coercive foce, Fe-Pt or Co-Pd type L1o phase nanoparticles are directly used as CNT growth catalyst, the size of which can be gradually reduced during CVD growth by sputter etch process toward ideal size regime.

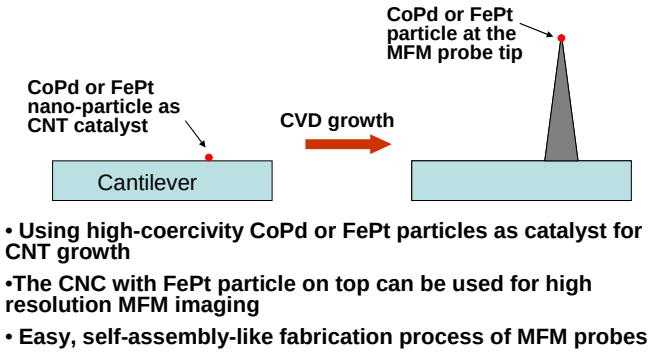

Fig. 12. Direct fabrication of high-resolution MFM tips with high coercivity L1o particles positioned at the MFM probe tip.

Shown in Fig. 13 and 14 are such MFM probe tips with ~12 nm diameter Co-Pd alloy (L1o phase) nanoparticles, and 10 – 15 nm diameter magnetic Ni nanoparticle at the tip of CNT.

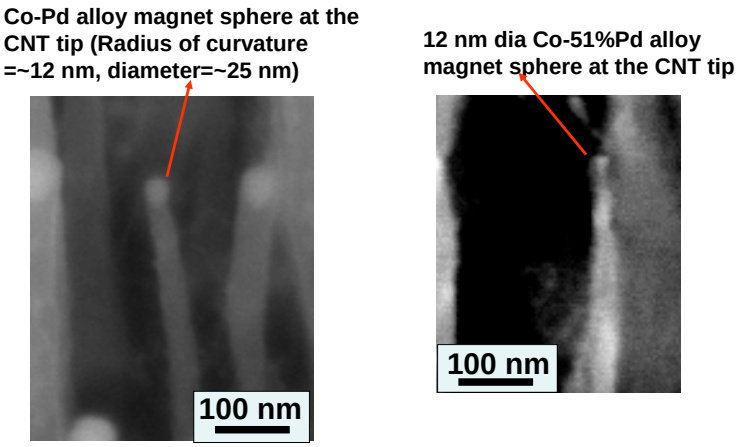

Fig. 13 Carbon nanotube tip with ~12 nm Co-Pd alloy nanoparticle at the apex of the CNT.

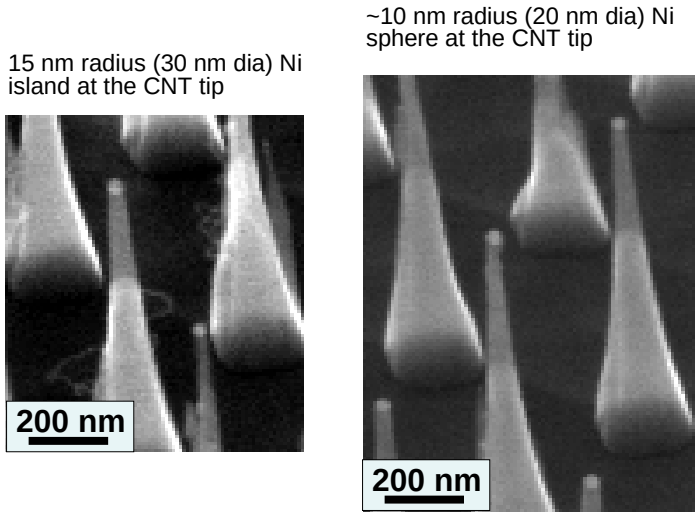

Fig. 14 Carbon nanotube tip with (a) ~15 nm diameter magnetic nanoparticle (Ni) at the tip, and (b) ~10 nm diameter Ni nanoparticle (Ni) at the tip in an array confuration.

AFOSR/AOARD

NBIT Program Phase I (2007-2010)

Part II

Final Report for Year 2

(May 2008 – Apr 2009)

Chapter 1

Title: **"SiGe Alloy Nanowire Photonics"**

Principal Investigator:

Prof. Moon-Ho Jo, Department of Materials Science and Engineering, POSTECH, Korea

Telephone: +82-54-279-2158

Facsimile: +82-54-279-2399

E-mail: mhjo@postech.ac.kr

Contract Number: FA4869-01-4048

AOARD Reference Number: AOARD-084048

AOARD **Program Manager:** Lt Col John Seo

Period of Performance: 2 year

Submission Date: 27 Aug 2009

Progress Report, Final-Term:

"SiGe Alloy Nanowire Photonics"

October 6 2008

Principal Investigators:

- Korean PI: Prof. Moon-Ho Jo, Department of Materials Science and Engineering, POSTECH, Korea

- US PI: Prof. Hongkun Park, Department of Chemistry and Chemical Biology, Harvard University, United States

Research Achievements:

1. Growth and doping of $Si_{1-x}Ge_x$ nanowires for the unit optical components:

- Journal Article: *Applied Physics Letters* **91**, 033104 (2007): "Fabrication of $Si_{1-x}Ge_x$ alloy nanowire field-effect transistors" by Cheol-Joo Kim, Won-Hwa Park, Jee-Eun Yang, Hyun-Seung Lee, Sunglyul Maeng, Zee Hwan Kim, Hyun M. Jang and **Moon-Ho Jo**

- Summary: We present the demonstration of nanowire field-effect transistors incorporating group IV alloy nanowires, $Si_{1-x}Ge_x$. Single-crystalline $Si_{1-x}Ge_x$ alloy nanowires were grown by a Au catalyst-assisted chemical vapor synthesis using SiH_4 and GeH_4 precursors, and the alloy composition was reproducibly controlled in the whole composition range by controlling the kinetics of catalytic decomposition of precursors. Complementary *in situ* doping of $Si_{1-x}Ge_x$ nanowires was achieved by PH_3 and B_2H_6 incorporation during the synthesis for *n*- and *p*-type field-effect transistors. The availability of both *n*- and *p*-type $Si_{1-x}Ge_x$ nanowire circuit components suggests implications for group IV semiconductor nanowire electronics and optoelectronics.

2. Growth of metallic nanowires for the optical device application (field-emission displays):

- Journal Article: *Advanced Materials* **19** 3637 (2007), "Spontaneous chemical vapor growth of NiSi nanowires and their metallic properties", Cheol-Joo Kim, Kibum Kang, Yun Sung Woo, Kyung-Guk Ryu, Heesung Moon, Jae-Myung Kim, Dong-Sik Zang and **Moon-Ho Jo**.

- Summary: We reported a simple and controlled synthesis at low temperatures of where single-crystalline NiSi nanowires by SiH_4 chemical vapor deposition (CVD) on Ni thin films predeposited on various substrates, such as SiO_2/Si, quartz, and indium tin oxide (ITO) substrates. The dimensionality of the Ni-silicides have been reproducibly directed from thin films to single-crystalline nanowires, as well as their phases, by fine-tuning of growth parameters during CVD of a SiH_4 gas precursor on predeposited Ni thin films. Single crystalline NiSi nanowires in this study exhibit typical metallic behaviors, and show promising field-emission properties. It is suggested that our simple method to spontaneously grow NiSi nanowires at low temperatures can provide a practical strategy to fabricate metallic nanostructures based on bottom-up synthetic approaches.

3. Characterizations of individual $Si_{1-x}Ge_x$ nanowires:

- Journal Article: *Applied Physics Letters* **91**, 223107 (2007): "Soild-phase epitaxy of amorphous Si using single-crystalline Si nanowire templates", Yun Sung Woo, Kibum Kang, Jong-Myeong Jeon, **Miyoung Kim** and **Moon-Ho Jo.**

- Summary: We report solid-phase epitaxy of amorphous Si *a*-Si shells using crystalline Si *c*-Si nanowire cores as seed templates. The *c*-Si core/*a*-Si shell nanowire heterostructures were *in situ* synthesized via a two-step chemical vapor deposition: the Au-catalytic decomposition of SiH4 for the core *c*-Si nanowires and the subsequent homogeneous decomposition of SiH4 at higher temperatures for the *a*-Si shells. Upon thermal annealing above 600 °C, the *a*-Si shells crystallize into *c*-Si shells from *c*-Si core nanowires in an epitaxial fashion. We discuss the crystallization kinetics of *a*-Si shells within the frame of Gibbs-Thomson effects arising from the finite size of nanowire seeds.

4. Growth and characterization of metallic nanowires for the optical device application (field-emission displays):

- Journal Article: *Nano Letters* **8** 431 (2008): "The Role of NiO Overlayers on Spontaneous Growth of $NiSi_x$ Nanowires from Ni Seed Layers", Kibum Kang, Sungkyu Kim, Cheol-Joo Kim, and **Moon-Ho Jo.**

- Summary: We report a controllably reproducible and spontaneous growth of single-crystalline $NiSi_x$ nanowires using NiO_x/Ni seed layers during SiH_4 chemical vapor deposition (CVD). We provide evidence that upon the reactions of SiH_4 (vapor)-Ni seed layers (solid), the presence of the NiO_x overlayer on Ni seed layers plays the key role to promote the spontaneous one-dimensional growth of $NiSi_x$ single crystals without employing catalytic nanocrystals. Specifically, the spontaneous nanowire formation on the NiO_x overlayer is understood within the frame of the SiH_4 vapor-phase reaction with out-diffused Ni from the Ni underlayers, where the Ni diffusion is controlled by the NiO_x overlayers for the limited nucleation. We show that single-crystalline $NiSi_x$ nanowires by this self-organized fashion in our synthesis display a narrow diameter distribution, and their average length is set by the thickness of the Ni seed layers. We argue that our simple CVD method employing the bilayers of transition metal and their oxides as the seed layers can provide implication as the general synthetic route for the spontaneous growth of metal-silicide nanowires in large scales**.**

5. Growth and characterization of axially composition modulated $Si_{1-x}Ge_x$ nanowires for the unit optical components:

- Journal Article: *Applied Physics Letters* **92**, 263111 (2008): "Axially graded heteroepitaxy and Raman spectroscopic characterizations of $Si_{1-x}Ge_x$ nanowires", Jee-Eun Yang, Won-Hwa Park, Cheol-Joo Kim, Zee Hwan Kim, and **Moon-Ho Jo.**

- Summary: We report the axially graded heteroepitaxy of $Si_{1-x}Ge_x$ nanowires, by the kinetic controls of the Au-catalytic decomposition of precursors during chemical vapor syntheses. Transmission electron microscope studies demonstrate that the relative composition of Si and Ge is continuously graded along the uniformly thick nanowires, sharing the same crystal structures with the continuously varying lattices. We also employed a confocal Raman scattering imaging technique, and showed that the local variations in Raman phonon bands, specific to Si and Ge alloying (ν_{Si-Si}, ν_{Si-Ge}, and ν_{Ge-Ge}) can be spatially and spectrally resolved along the individual nanowires, within the spatial resolution of ~500 nm.

6. Large area growth of Ge nanowires:

- Journal Article: *Advanced Materials* Accepted for Publication (2008): "Low-Temperature Deterministic Growth of Ge Nanowires Using Cu Solid-Catalysts", Kibum Kang, Dong-An Kim, Hyun-Seung Lee, Cheol-Joo Kim, Jee-Eun Yang and **Moon-Ho Jo.**

- Summary: We report the low-temperature growth of Ge NWs by using Cu-catalysts at as low as 200 °C in a deterministic manner, so that the diameter of Ge NWs is uniformly distributed at 7 nm, directly templated from the identical size of Cu

catalysts, with the consistent [011] crystallographic orientation. Specifically it was found that the Cu catalyst tips are consistently orthorhombic Cu3Ge with the heteroepitaxial relation with the cubic Ge NWs, as [010]tip//[011]NW, along the wire axes. We attribute the low-temperature growth of 200 °C, which is well below the Cu-Ge eutectic temperature of 644 °C, to the growth by the catalytic decomposition of Ge precursors onto the solid-phase Cu catalysts, and describe distinct manifestations of the solid-catalytic growth from the parallel comparison to the growth from the eutectic liquids catalysts. We further demonstrate that the solid-catalytic growth in our study can be readily adapted for the vertical growth by an epitaxial manner on Si substrates. We argue that the low-temperature growth of semiconductor NWs using the solid catalysts can be generally accessible, provided that the appropriate combination of solid catalysts and semiconductors are thermodynamically available, thus suggest implication for the potential large-area integrated growth on various substrates.

Collaborative Team Efforts:

1. Program kick-off meeting: June 4-5 2007, Seoul Korea by both KPI and USPI

2. Research training of a graduate student (Cheol-Joo Kim from KPI) at the USPI Lab: Jul 19-27 2007

: Collaboratively developed and bench-marked individual nanowire optoelectronic measurement set-ups:

Optoelectronic measurement set-ups

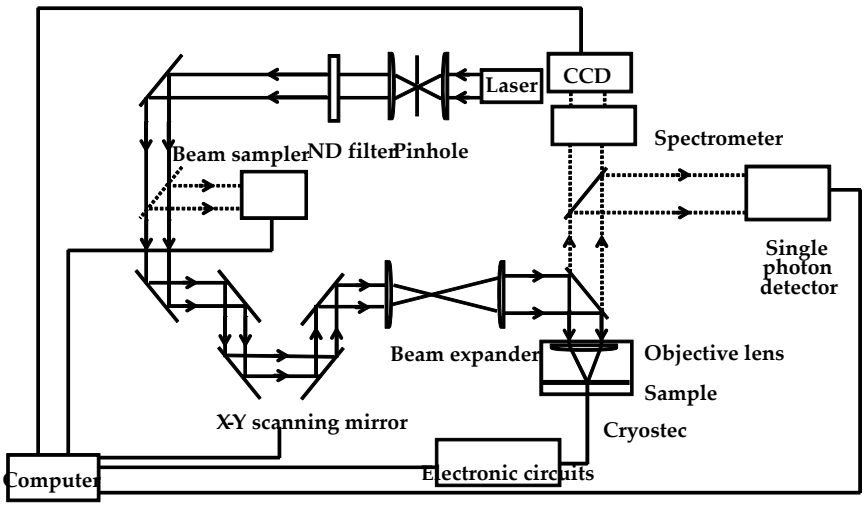

3. The 1st Team Meeting: Jul 19-21 2007, Harvard University, US (KPI-USPI)

4. US researcher (Dr Myung-Han Yoon from USPI) visit to KPI's Lab: Nov 13 2007

5. The 2nd Team Meeting: Dec 4-7 2007, Seoul, Korea (KPI-USPI)

6. Research training of a graduate student (Hyun Seung Lee from KPI) at the USPI Lab: Jun 06 - Sep 07 2008

: Collaboratively characterized photoconductivity of $Si_{1-x}Ge_x$ nanowire devices:

7. The 3rd Team Meeting: Aug 7-8 2008, Seoul, Korea (KPI-USPI)

Team Achievements:

- *Applied Physics Letters* **91**, 223107 (2007): "Solid-phase epitaxy of amorphous Si using single-crystalline Si nanowire templates", Yun Sung Woo, Kibum Kang, Jong-Myeong Jeon, Miyoung Kim and Moon-Ho Jo**.**

- *2008 Gordon Conference*, (July 27 - August 1, 2008 Tilton, NH, US): Plasmonics, Optics At The Nanoscale, "Electrical Detection of Surface Plasmons in the Near Field", Abram L. Falk, Frank H. Koppens, Chun Yu, Nathalie de Leon, Kibum Kang, Moon-Ho Jo, Mikhail Lukin, Hongkun Park

- Article in preparation: "Near-Field Electrical Detection of Guided Surface Plasmons", Abram L. Falk, Frank H. Koppens, Chun Yu, Kibum Kang, Nathalie de Leon , Alexey Akimov, Moon-Ho Jo, Mikhail Lukin, and Hongkun Park

Chapter 2

Title: **"Self-Assembled Liquid Crystalline Gels: From Nanostructure to Function"**

Principal Investigator:

Prof. Soo-Young Park, Department of Polymer Science, Kyungpook National University, Korea

Telephone: +82-53-950-5630

Facsimile: +82-53-950-6623

E-mail: psy@knu.ac.kr

Contract Number: FA4869-01-4048

AOARD Reference Number: AOARD-084048

AOARD **Program Manager:** Lt Col John Seo

Period of Performance: 2 year

Submission Date: 24 Aug 2009

Annual Progress Report

Collaborative research between KNU and Caltech on new materials formed from block copolymers and small molecule liquid crystals (LCs) during Years 1 and 2 of the AFOSR-MOST has included:

- Surprising discoveries during fundamental studies of the conformations of dilute solutions of side-group liquid crystalline (SGLCP) homopolymers with different modes of attachment ("end-on" and "side-on"), which guide the design of LC-coil block copolymers for future applications [Caltech].
- Synthesis of both deuterated and non-deuterated coil-LC di- and tri-block copolymers [KNU].
- Exploration of the self-assembly of coil-LC diblock copolymers in small molecule LC solvent [KNU and Caltech].
- Culminating in demonstration of responsive LC-coil block copolymers for switchable interfacial organization at LC-air and LC-water interfaces [KNU and Caltech].

These results and their relationship to our overarching goals are described below.

Side-group liquid crystal polymers (SGLCPs), flexible-chain polymers functionalized with liquid crystalline (LC) side-groups, exhibit unique properties that arise from the coupling of the orientational order inherent in the LC side group to the flexible backbone of the polymer.[1,2] In contrast to random coil polymers, SGLCPs adopt an anisotropic conformation upon dissolution in a small-molecule LC. Block copolymers with side-group LC midblocks and LC-phobic endblocks spontaneously form gels under conditions that cause the end-blocks to reject the solvent; this gelation is reversible, opening new opportunities for processing the materials. In contrast to *in-situ* polymerized networks, these physical gels are homogeneous systems. Consequently, the gels have exceptional clarity and their response to stimuli, such as change in temperature or electric field, is sharp—overcoming two of the major deficiencies of prior LC elastomers and gels. Our collaboration addresses the need for structure-property relationships that connect the molecular structures of the polymer and LC solvent with the nanostructure that they spontaneously form, and between the nanostructure and macroscopic properties.

Caltech:

Side Group Liquid Crystal Homopolymers

During Year 1 we tested the electro-mechanical-thermodynamic effects of changing the length and type of the flexible spacer linking the mesogenic side groups to the polymer

backbone (Figure 1). In Year 2 we continued our study of the structure and conformation of SGLCP homopolymers to further understand the SGLCP nanostructure in small molecule LC solvent.

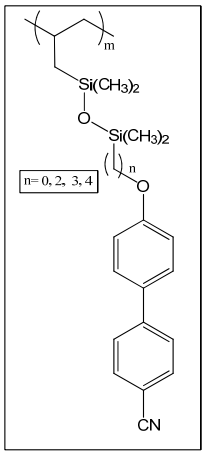

.

Figure 1. In Year 1 of the AFOSR-MOST we synthesized and studied the structure and conformation of a series of end-on side group liquid crystal polymers with differing spacer lengths.

In Year 2 of our AFOSR-MOST collaboration, we made two exciting discoveries during Small Angle Neutron Scattering (SANS) experiments at NIST's NCNR while characterizing two families of SGLCPs in small molecule LC solvent. The two families of SGLCPs under investigation have profoundly different orientational coupling between their liquid crystal mesogens and their polymer backbones: the "end-on" SGLCP (Figure 2a) adopts a mildly oblate conformation, while the "side-on" SGLCP (Figure 2b) adopts a strongly prolate conformation, in both cases the symmetry axis coincides with the director[3]. The Kornfield lab has synthesized both end-on and side-on SGLCP homopolymers, in order to isolate the orientational behavior of the SGLCP blocks. Small angle scattering is ideal for studying the conformational and orientational behavior of these SGLCPs, and SANS, in particular, was essential due to insufficient contrast seen in earlier x-ray (SAXS) experiments.

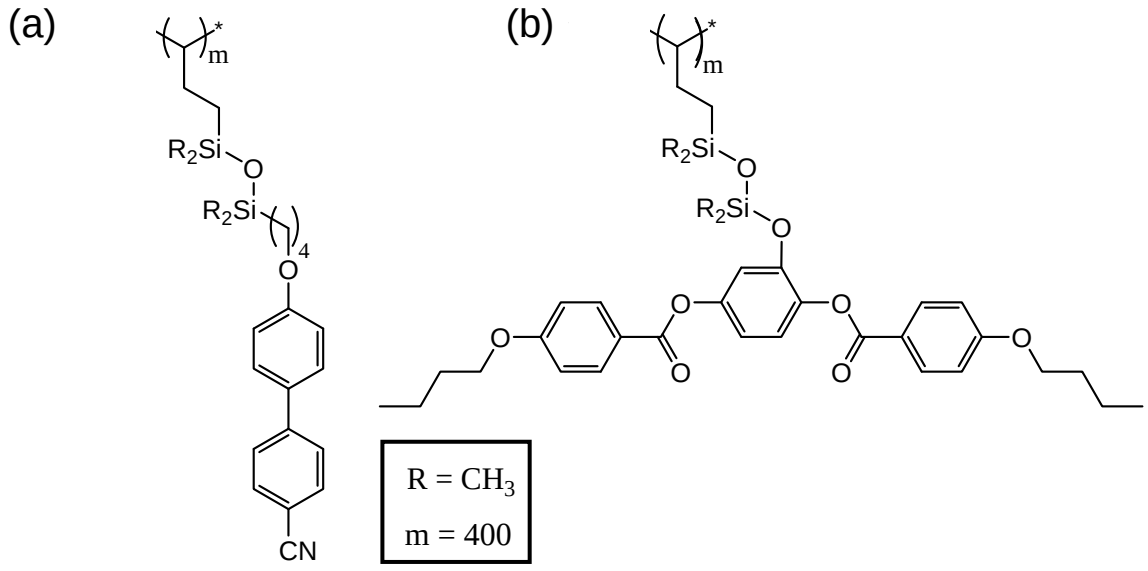

Figure 2. Our homopolymers have liquid crystalline side groups either (a) terminally attached, or "end-on" and (b) laterally attached, or "side-on" SGLCP blocks.

Our previous studies of these homopolymer solutions (at 5wt% polymer in small molecule LC) in an aligned nematic phase show 2D SANS patterns characteristic of oblate ($R_{\parallel}/R_{\perp} \approx 1.6$) ellipsoidal conformation for the end-on SGLCP (Figure 3a, top) and prolate($R_{\parallel}/R_{\perp} \approx 4.5$) for the side-on homopolymers (Figure 3a, bottom)[4]. The dimensions deduced from these patterns showed that the coils were overlapping, motivating experiments at still lower concentrations, to determine the dimensions of the individual coils. The 2D SANS patterns obtained at 1wt% polymer yielded a surprising new feature: an intense streak oriented along the director which is very strong at low q (Figure 3b). This suggests a long-range interaction that biases the pair-pair distribution of the chains; however, the long range interactions now familiar for colloidal particles in a small molecule nematic cannot describe the observed orientation of the streak (in colloids, particles tend to form lines along the director, which would in turn result in a streak perpendicular to the director in the 2-D SANS patterns). Instead, we believe this streak is the result of fluctuation mediated Casimir-like attraction of the (individual polymer chains) perpendicular to the director[5]. The SGLCPs do not disturb the orientation of the director; rather, they perturb the fluctuations of the director. This explains the orientations of the streak as well as why it retains this orientation for both oblate and prolate SGLCPs. To our knowledge this effect has never been reported before and it motivates further experiments in future years of the AFOSR-MOST program.

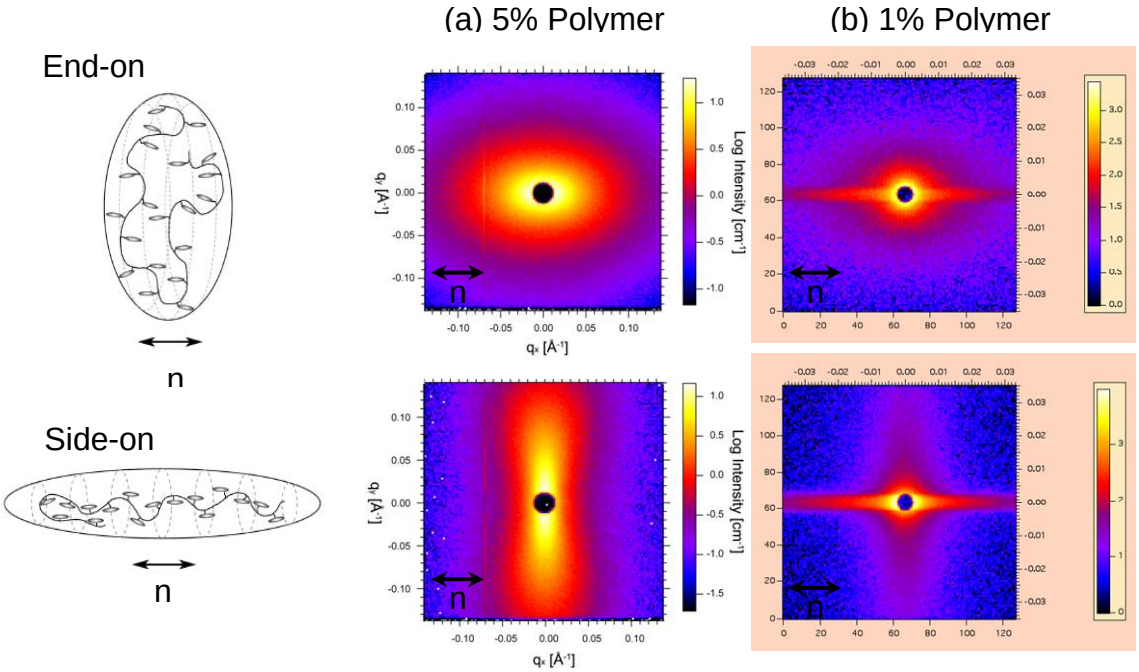

Figure 3. 2-D SANS patterns at low q for (a) 5% by weight of the end-on and side-on homopolymers in the nematic phase and (b) 1% by weight, or below the overlap concentration, of the end-on and side-on

homopolymers in the nematic phase. The patterns are of from longest detector distances (13m and 11m) available for NG5 and NG3, respectively.

In order to extract the size and configuration that the polymer assumes under these conditions, we are in the process of developing data analysis tools to facilitate quantitative understanding of the 2-D scattering patterns. These include iso-intensity plots (Figure 4) and azimuthal scattering intensity variation at specific q regimes (Figure 5). This will enable us to explicitly correlate the anisotropic effects with a polymer configuration, molecular weight and the orientation of the LC mesogen with respect to the backbone. We are also developing a method for fitting an ellipsoidal object to the data in order to extract the shape that best represents the polymer chains.

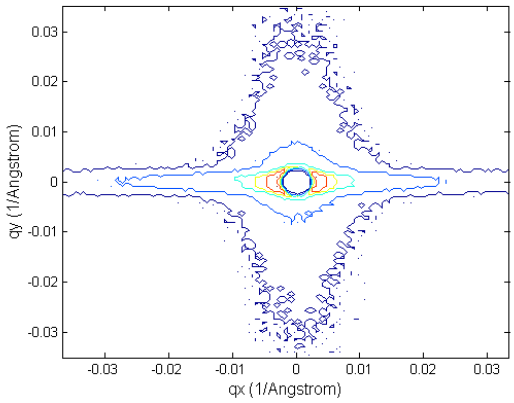

Figure 4: Iso-Intensity plot of 48kBB at 20 degrees C, obtained at a sample to detector distance of 11 meters. The contours correspond to intensities. I=20, 100, 500, 1000, 2000, 8000 (from high to low q)

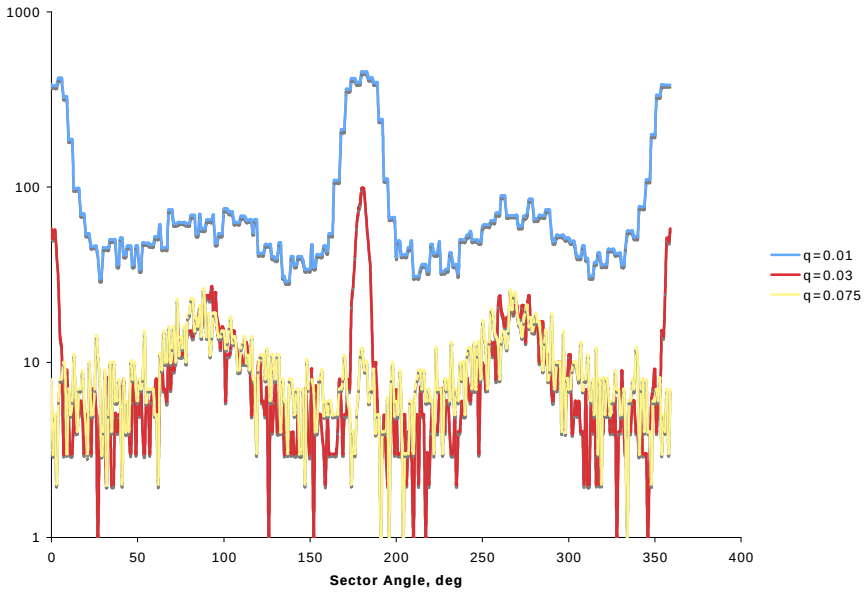

Figure 5: Azimuthal Intensity Variation plot of 48kBB at 20 degrees C, obtained at a sample to detector distances of 11 meters and 4.5 meters as corresponding to appropriate q values.

Pre-transitional Effect of Dilute Solutions of Side-on Homopolymer

When the 1% polymer samples were heated to temperatures above, but close to the nematic-isotropic transition temperature (T_{ni}) of the LC solvent, another surprise emerged. When the solvent switches from nematic to isotropic, 2D SANS patterns generally become isotropic (as is reported in all prior literature). However in our polymer with the strongest anisotropy (side-on), *anisotropy persisted above the* T_{ni} (T_{ni} +2, Figure 6) in the mid and high q regimes. It is possible that the polymer creates an "internal nematic field" resulting in local ordering of the small molecule LC within/around the polymer, similar to the way certain boundary conditions can locally condense isotropic LC into the nematic phases above the bulk T_{ni} (capillary condensation)[6]. Additional experiments indicated that the magnetic field does not induce the effect; it breaks symmetry – making it possible to observe the effect. Again, to our knowledge this effect has not been reported and further probing of this unexpected finding with different molecular weights of this polymer in the small temperature region above the T_{ni} can help us elucidate this phenomenon.

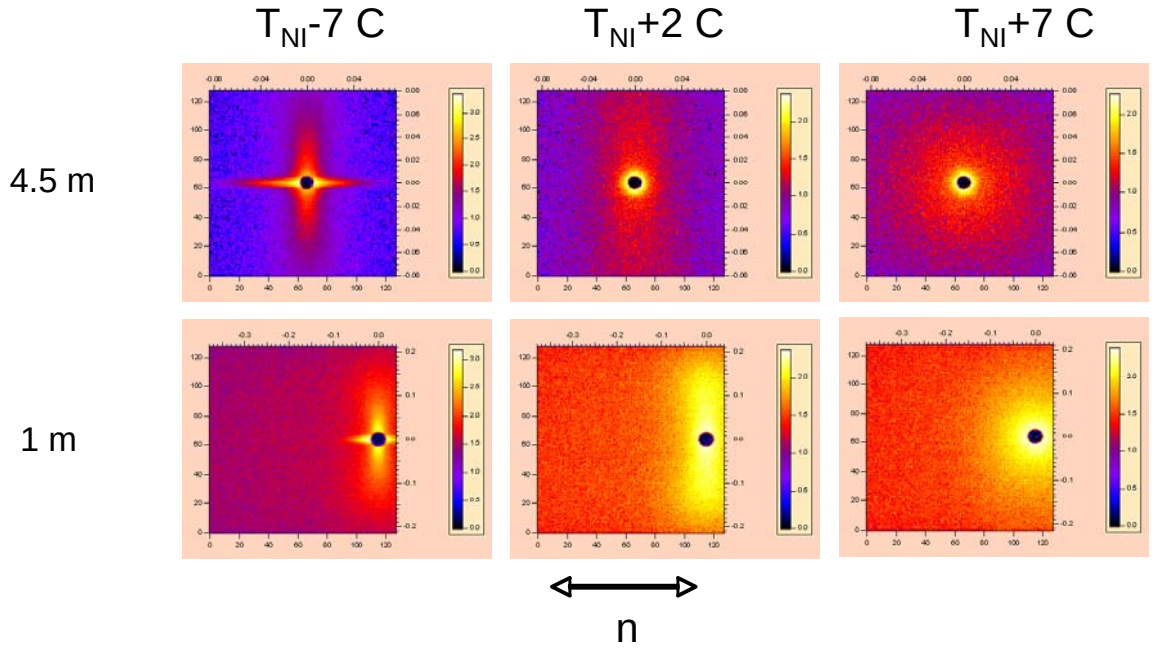

Figure 6. 2-D SANS patterns of the side-on homopolymer across the nematic-isotropic transition in the mid and high-Q regimes. Data were obtained at 20 °C, 29 °C and 34 °C. T_{NI} ~ 27 °C.

Coil-SGLCP diblock Copolymers

We have also carried out SANS of coil-LC diblock copolymers (Figure 7), both at NIST and at LANCSE. As seen in Figure 8, the azimuthally averaged 1-D SANS data for the side-on coil-LC diblock copolymer in 5CB shows the presence of a Guinier regime in the isotropic temperature regime (29 C and 34C). The dimensions extracted from a Guinier Analysis agree well with direct, visual confirmation of these structures as seen via Transmission Electron Microscopy (TEM), Figure 9. (These measurements build on the initial TEM characterizations carried out both by students in the Park lab, and by a joint effort of both Caltech and Kyungpook students, in Year 1 of this grant).

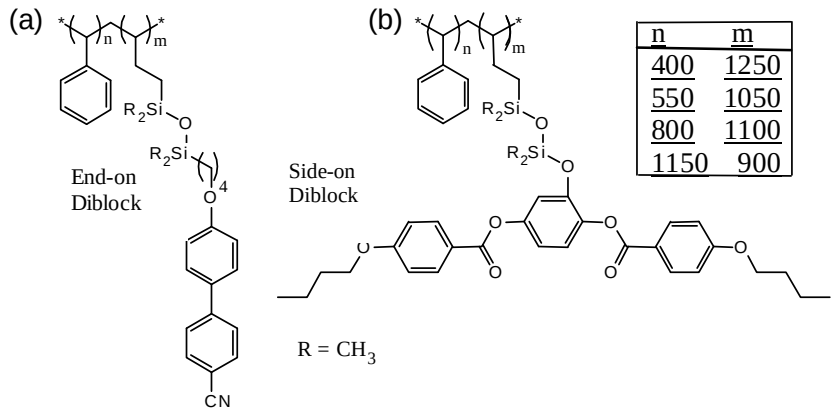

n	m
400	1250
550	1050
800	1100
1150	900

Figure 7. Our diblocks are made up of a polystyrene coil block and either (b) terminally attached, or "end-on" and (b) laterally attached, or "side-on" SGLCP blocks. The diblocks have approximately constant SGCLP content, *m*, while their polystyrene content, *n*, varies across the series from less than that of the SGLCP to more than that of the SGLCP[7].

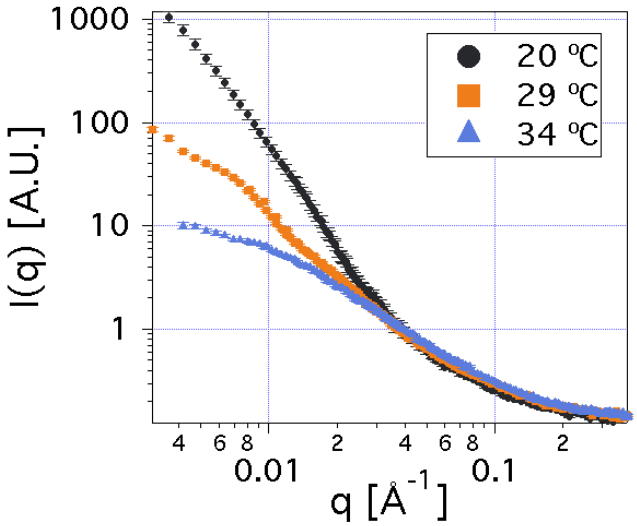

Figure 8: Azimuthally averaged 1-D SANS data from the side-on PS-SGLCP at T_{ni}-7ºC (20ºC), T_{ni}+2ºC (29ºC) and T_{ni}+7ºC (34ºC). The degree of polymerization of the coil (PS) and the LC sections are n=1150 and m=900, respectively.

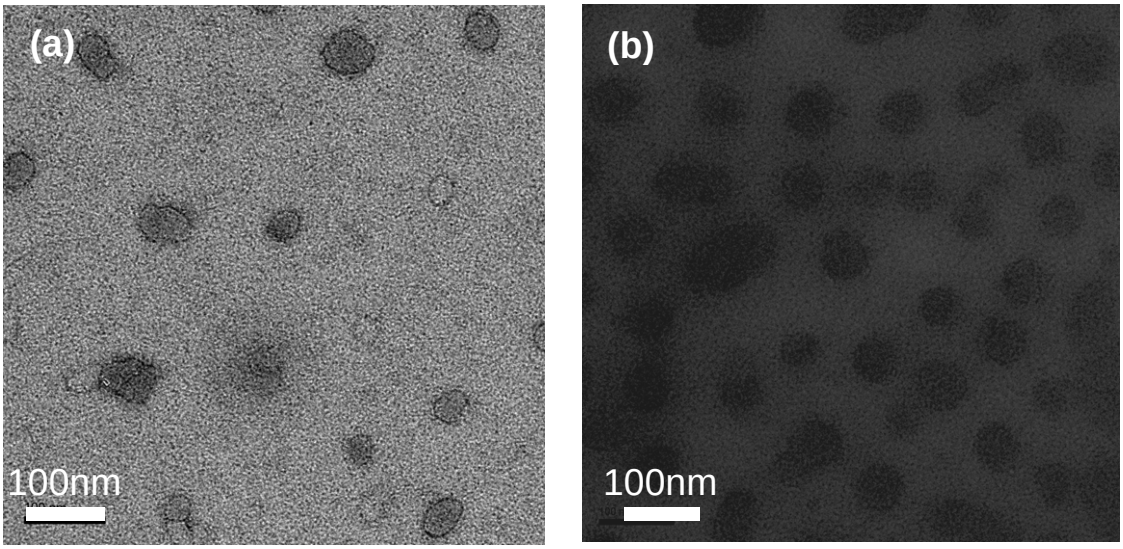

Figure 9: Unstained TEM micrographs of 0.5 wt% (a) side-on and (b) end-on PS-SGLCP (n = 1150, m = 900, for both cases) in 5CB. Solutions were cast on a carbon-coated Cu grid and dried under ambient conditions.

These techniques probing the reciprocal and real space indicate larger structures than would be expected of typical block copolymers in selective solvents. For example, Lodge[7] and Register[9] found micelle diameters in the range of 10-20nm for polystyrene-*b*-polyisoprene diblocks of comparable molecular weights in selective solvents, while the diameters seen in the micrographs of our SGLCP system are on the order of 50-100nm. Furthermore, the distribution of sizes seen in the TEM micrographs of the diblock copolymers is suggestive of possible vesicular structures. We have applied for further SANS time to continue these investigations.

KNU:

Summary:

In the 2nd year, we prepared the PS-*b*-LCnP diblock and LCnP-*b*-PS-*b*-LCnP triblock copolymers using an ATRP (atom transfer radical polymerization) method. Following is summary of the 2nd year work

Synthesis of PS-*b*-LCnP diblock copolymers and LCnP-*b*-PS-*b*-LCnP triblock copolymers

Synthesis of Me_6[14]aneN_4 as a ligand 5,5,7,12,12,14-hexamethyl-1,4,8,11-tetraazamacrocyclotetradecane (Me_6[14]aneN_4) was prepared according to Scheme 1,[8] and was confirmed by NMR (Fig 10)

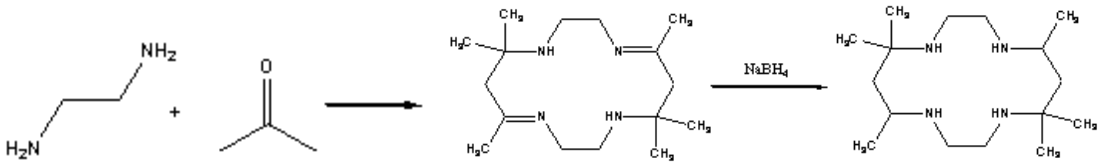

Scheme 1. Synthesis of Me_6[14]aneN_4

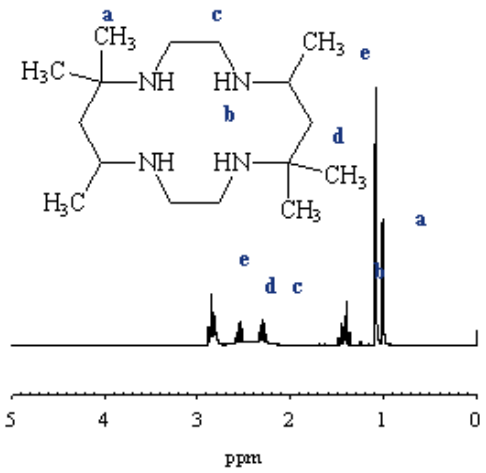

Figure 10. 1H-NMR spectra of Me_6[14]aneN_4

Polymerization of PS-Br macroinitiator by ATRP. CuBr and magnetic bar were added into a Schlenk flask. The flask was degassed by four vacuum-N_2 cycles. *N*,*N*,*N'*,*N'*,*N''*-pentamethyldiethylenetriamine (PMDETA), styrene monomer and 1-phenyl ethyl bromide (1-PEBr) were previously degassed by bubbling N_2 through it for 30 min, were then introduced into the flask using a syringe purged with nitrogen. The flask was then placed in an oil bath previously heated to 110℃. After specified polymerization time, the resulting polymer was dissolved in THF, and passed through alumina column. After that it was concentrated by rotary evaporator and precipitated in methanol several times. The white polymer was dried under vacuum at 50℃ for 10hr.

Polymerization of PS-*b*-LCnP diblock copolymer by ATRP. CuBr, LCn monomer, PS-Br macroinitiator, and magnetic bar were added into a Schlenk flask. The flask was degassed by four vacuum-N_2 cycles. Me_6[14]aneN_4 as ligand, and anisole as solvent were previously degassed by bubbling N_2 through it for 30 min, were then introduced into the flask using a syringe purged with nitrogen. The flask was then placed in an oil bath previously heated to 80℃. After reasonable polymerization time, the resulting polymer was dissolved in THF, and passed through alumina column. After that it was

concentrated by rotary evaporator and precipitated in methanol several times. The white polymer was dried under vacuum at 50℃ for 10hr.

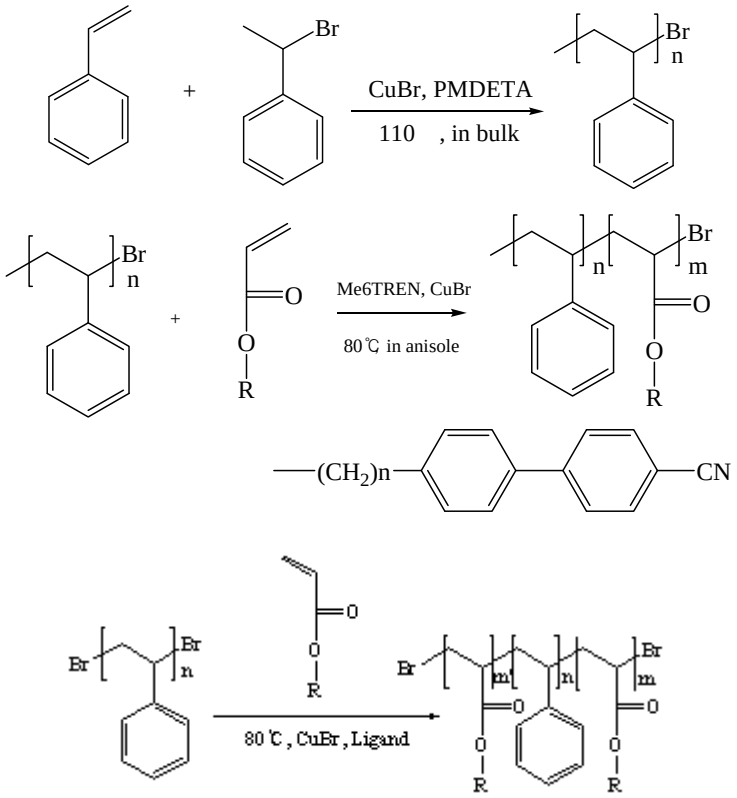

Scheme 2. Polymerization of PS-*b*-LCnP and LCnP-*b*-PS-*b*-LCnP block copolymers

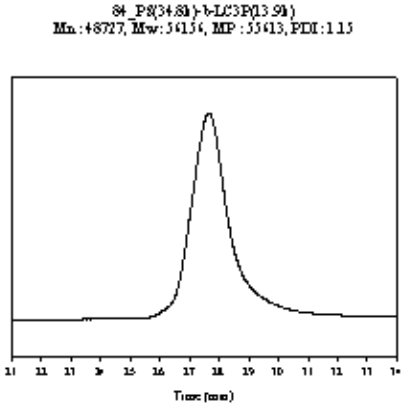

Sample	Mn	Mw	PDI (Mn/Mw)	DPn of LC
PS(34.8k)-b-LC3P	48727	56156	1.15	**45**

Figure 11. GPC result of PS-*b*-LC3P

SANS study

We prepared PS-b-LCnP diblock, and LCnP-b-PS-b-LCnP triblock copolymers with narrow polydispersity index (Figure 11). But micelle measurements of these block copolymers with Small Angle X-ray Scattering (SAXS) is difficult, because there is little electrical density difference between micelle and 5CB as a solvent Therefore, we prepared dPS-Br and Br-dPS-Br as macroinitiators with deuterated styrene monomer

collaborating with CNMS at Oak Ridge National Laboratory. dPS-b-LCnP and LCnP-b-dPS-b-LCnP were successfully polymerized with these dPS macroinitiators. To study SANS, we prepared 1 wt% of block copolymer solutions in nematic LC small molecule, 5CB (selective solvent of LCnP block). From Figures 12 and 13, we can assume that micelle was formed with dPS block as core and LCP block as corona. To examine more closely, we will do a 2nd SANS experiment.

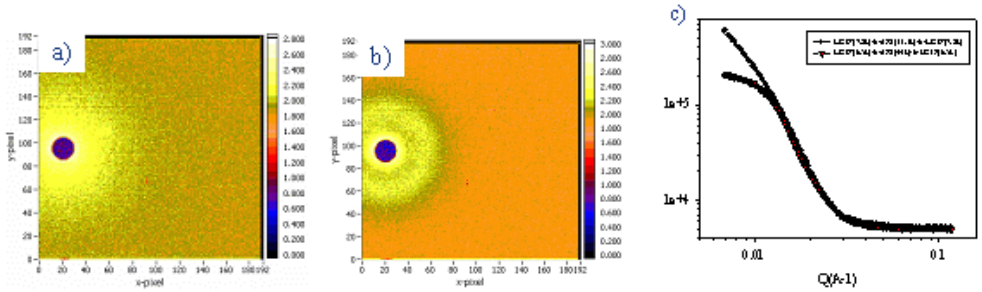

Figure 12. SANS results of solution of LC3P-b-dPS-b-LC3P in 5CB (1 wt%)

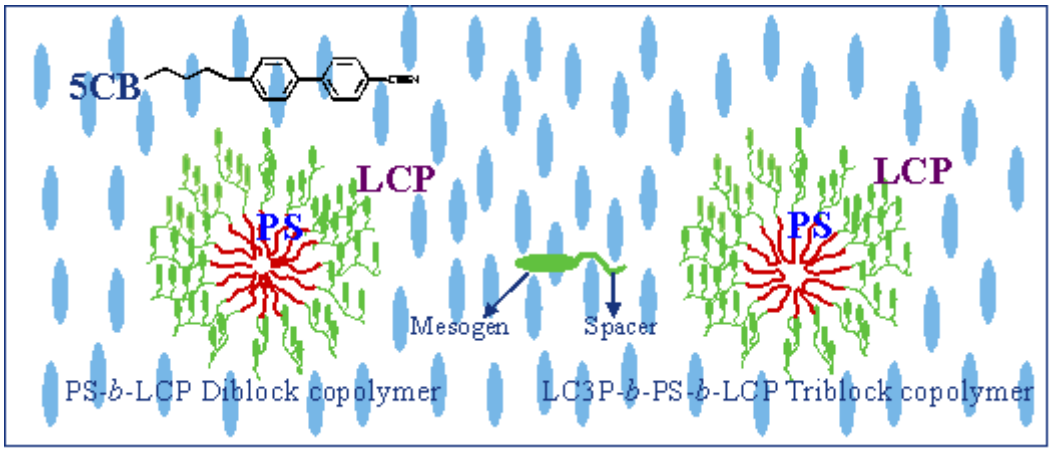

Figure 13. The illustration of micellar structure of LCnP-b-dPS-b-LCnP in 5CB

Optical Properties Study

PS-b-LCnP block copolymers were observed by melting between slide glasses at cross polar state of polarized optical microscope. In the cases of LC6P and LC11P, both homo and block copolymers showed LC texture below TNI. However, LC3P did not show LC phase, because the length of alkyl chain as a spacer was too short, and thus mobility of the mesogen was limited. We confirmed that LC block copolymer has TNI by DSC (Figure 15) and above TNI, it showed isotropic state (Figure 14c).

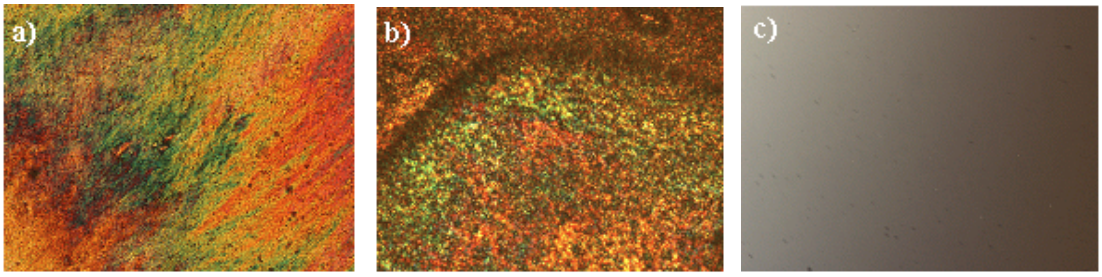

Figure 14. Polarized optical images of (a) PS-b-LC11P, (b) PS-b-LC6P block copolymer at room temperature and (c) at 160°C

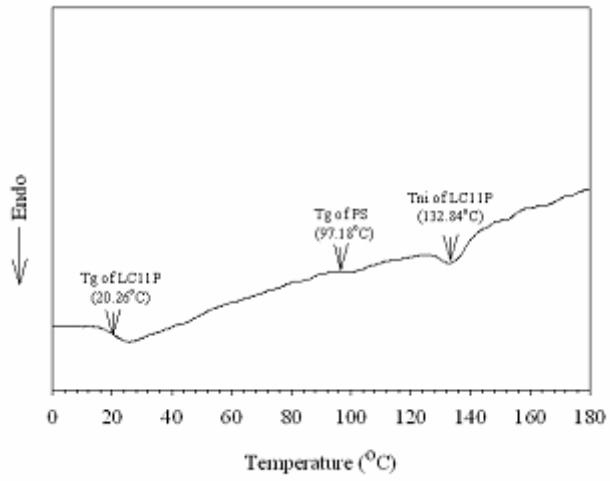

Figure 15. DSC traces of PS-b-LC11P diblock copolymer

Future Work

Year 3 of the AFOSR-MOST KNU will build on the homopolymer studies carried out at Caltech and the conformation studies and polymer synthesis carried out at KNU to rationally design block copolymer systems that have a scientific impact and many potential applications. Using results obtained in Year 1 and 2, emulsions and dispersions of SGLCP block copolymers will be studied both at their interface with air or water and for their unique phase behavior in selective solvents. Specifically, we hope to test the crew-cut diblock copolymers synthesized by the Park group at KNU with interface measurements initiated by the Kornfield group at Caltech. Further SANS studies by both parties will also increase our knowledge about the conformation of this interesting class of materials when they are dissolved in small molecule liquid crystals.

---

[1] Kempe, M. D.; Kornfield, J. A.; Lal, J. *Macromolecules* **2004**, *37*, 8730-8738.

[2] Kempe, M. D.; Kornfield, J. A. *Physical review letters* **2003**, *90*, 115501-115501.

[3] Kempe, M. D.; Scruggs, N. R.; Verduzco, R.; Lal, J.; Kornfield, J. A. *Nature Materials* **2004**, *3*, 177-182.

[4] Ibid, 177.

[5] Bartolo, D.; Long, D.; Fournier, J. B. *Europhysics Letters* **2000**, *49*, 729-734.

[6] Bracic, A. B.; Kocevar, K.; Musevic, I.; Zumer, S. *Physical Review E* **2003**, *68*.

[7] Lodge, T.P. Pudil, B: Hamley, K.J. *Macromolecules*, **2002**, *35*.

[8] Bodie ED, editor. Inorg. Synth., vol 18. New York: John Wiley; 1978.

Chapter 3

Title: **"Extremely Low Noise CNT for Peltier and Photo-Detector Device Application"**

Principal Investigator:

Prof. Young-Hee Lee, Department of Physics, SungKyunkwan University, Korea

Telephone: +82-31-299-6507

Facsimile: +82-31-299-6505

E-mail: leeyoung@skku.edu

Contract Number: FA4869-01-4048

AOARD Reference Number: AOARD-084048

AOARD **Program Manager:** Lt Col John Seo

Period of Performance: 2 year

Submission Date: 27 Aug 2009

NBIT PROGRAM 2007-2010

Report

Part I. General Information	For KOSEF use only	

1. Project Title (in English): Extremely Low Noise Carbon Nanotubes for Peltier and Photo-detector Device Applications			
2. Research Code Number	200702	3. Sub-research field	nanophysics
4. Research Duration	From 20080401 To 20090331		

5. Applicant Information

Korean Principal Investigator (KPI)		US Principal Investigator (USPI)	
Full Name (age)	Young Hee Lee (54)	Full Name (age)	Moon J. Kim (45)
Nationality	Korea	Nationality	Korea
Affiliation (department)	Sungkyunkwan University (Department of Physics)	Affiliation (department)	University of Texas at Dallas (Department of Electrical Engineering)
Position	Professor	Position	Professor

Telephone	+82-31-299-6507	Telephone	+001-972-883-6635
Fax	+82-31-290-5954	Fax	+001-972-883-6629
E-mail	leeyoung@skku.edu	E-mail	moonkim@utdallas.edu
Address	440-746, 300 Cheoncheon-dong, Jangan-gu, Suwon, Korea	Address	EC 33, Box 830688 Richardson, Texas 75083-0688, U.S.A.

6. Authentication and Commitment

Korean Principal Investigator (KPI) Name Young Hee Lee Date 2009.08.22

MID-TERM REPORT

Task	Extremely Low Noise Carbon Nanotubes for Peltier and Photo-detector Device Applications
Korea Principal Investigator	Young Hee Lee, Ph. D. Sungkyunkwan University
U.S. Principal Investigators	Moon J. Kim, Ph. D. University of Texas at Dallas Minhee Yun, Ph. D. University of Pittsburgh
Report Period	April 07 to March 08

I. Progress Summary

In order to utilize carbon nanotubes for low noise thermal devices, precise control of doping is required. Several approaches have been tried:

~~2.~~ The position of chemical dopant, doping content, Fermi level engineering were achieved electrochemically by controlling gate bias and source-drain bias.

Formatted: Bullets and Numbering

- Air-stable n-type doping was realized by introducing viologen, revealing stability in air and water up to 100 days with high controllability of doping concentration.

- We proposed that the intrinsic ambipolarity of CNTs can be utilized for adaptive logic circuit and demonstrated the space saving, i.e., NOR and NAND functions by using the four transistors by simply chaing the input polarity. This was highlighted in Asia Materials published by Nature group.

- CNT transistors were modeled by various theories. In particular, by intentionally having electron beam irradiation on CNTs, hopping Poole-Frenkel model was introduced to fit metallic and semiconducting CNTs.

**** 14 journal papers have been published or accepted for publication**

Personal exchange Result

Internal(Korea) -> abroad

Item	Countries	Institution	Period	Researcher				Short-term/ Long-term
				nationality	name	degree	major	
Attend Conference	Singapore	Regional electrochemistry Meeting of South-East Asia conference	2008. 8.4 ~ 8.7	Korea	Woo Jong, Yu	Master's Course	Semiconductor	Short-term
Dispatch researcher	USA	University of Texas at Dallas	2008.3.5 ~5.22	Korea	Seong Chu, Lim	Doctor	Physics	Long-term
Dispatch researcher	USA	University of Pittsburgh	2007.10.13 ~10.21	Korea	Young Hee, Lee	Doctor	Physics	Short-term
Dispatch researcher	USA	University of Texas at Dallas	2007.9.29 ~10.05	Korea	Seong Chu, Lim	Doctor	Physics	Short-term

abroad -> internal(Korea)

item	visit institution	period	researcher				Short-term/ Long-term
			nationality	name	degree	major	
Consultant	Sungkyunkwan University	2008. 11. ~ 2008. 11	France	Didier Pribat	Doctor	Physics	Short-term
Dispatch researcher	Sungkyunkwan University	2008. 5~ 2008. 7	USA	Dave Perello	Master's Course	Electronics	Long-term
Dispatch researcher	Sungkyunkwan University	2008. 5~ 2008. 7	USA	Michael Nayhouse	Bachelor	Electronics	Long-term
Dispatch researcher	Sungkyunkwan University	2007. 6. 27 ~ 2007. 8. 28	USA	Dave Perello	Bachelor	Physics	Long-term

II. Significant Technical Progress at Sungkyunkwan University

II-A. Bias-induced doping engineering with ionic adsorbates on single-walled carbon nanotube thin film transistors

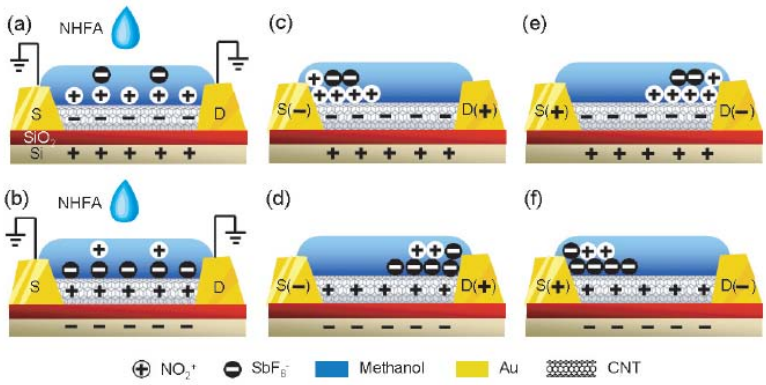

Figure 1. (a) and (b) While the NHFA solution is dropped, a gate voltage (Vg) of +10V or −10V is applied with grounded source–drain voltage. While applying Vg = +10 V, a drain bias (Vd) of (c) +1V or (e) −1V is applied. While applying Vg = −10 V, (d) Vd = +10 or (f) Vd = −10 V.

Figure 1 shows a schematic diagram demonstrating the concept of bias-induced doping by ionic adsorbates. For positive gate bias, CNTs are negatively charged and therefore the positively charged nitronium ions (NO^{+2}) are selectively adsorbed on the CNTs (figure 1(a)). Similarly, CNTs are positively charged with a negative gate bias, and henceforth negatively charged hexafluoroantimony (SbF^{-6}) ions are attached to the CNT surface (figure 1(b)). In order to selectively position the ionic adsorbates within the TFT, a drain bias (source being ground) is applied, while maintaining either a negative or positive gate bias. In the case of a positive gate bias and a positive (negative in figure 1(e)) drain bias, accumulation of NO^{+2} ions is much higher near the negatively charged source (drain in figure 1(e)) electrode than that of the SbF^{-6} ions, which mostly flow away (figure 1(c)). Similarly, depending on drain polarity, the SbF^{-6} ions are accumulated on the drain or source regions at a negative gate bias (figures 1(d) and (f)).

II-B. Reduction-Controlled Viologen in Bisolvent as an Environmentally Stable n-Type Dopant for Carbon Nanotubes

When this solution was dropped onto CNTs, V_0 molecules in the toluene region became oxidized by donating electrons to CNTs spontaneously and reached the V^{2+} state. This redox analyte undergoes a reversible two-electron redox reaction, as shown in Figure 2a. The large Gibbs free energy difference

of 2.4 kcal/mol between BV^{2+} and BV^{0} prevents BV^{2+} from being reduced to BV^{0} under ambient conditions. This could be a clue to providing environmental stability in doped CNTs which will be discussed later. The CNT-TFT prepared by PECVD in Figure 2b showed a clear p-type behavior with back-gate modulation (high current at negative gate bias and no current at positive gate bias). With a single drop of V^{0} solution in 5 mM, the carrier type was converted from p-type (hole carrier) to n-type (electron carrier), i.e., high on-current at positive gate bias and small offcurrent at negative gate bias (Figure 2c). This is ascribed to the electron donation to CNTs during the charge state conversion of viologen fromV^{0} toV^{2+}. The development of a Breit-Wigner- Fano (BWF) component at the lower energy side of the G-band in Figure 2d is further evidence of charge accumulation in CNTs. The inset also indicates phonon softening of the G-band by 2 cm^{-1}, which is additional evidence of a Fermi level shift in CNTs.

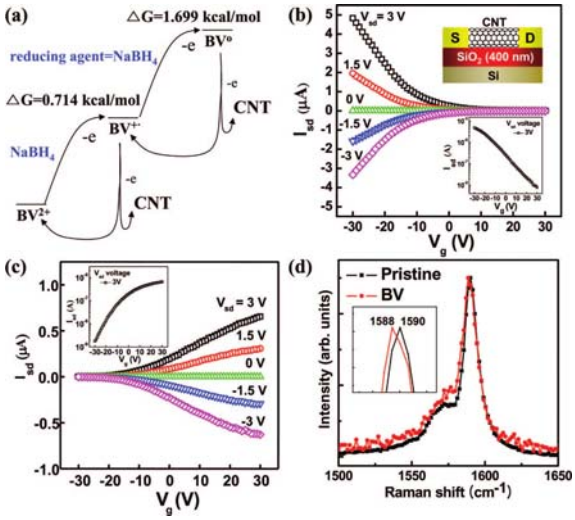

Figure 2. (a) Reversible redox reaction with Gibbs free energy difference. (b) Typical I-V characteristics of the pristine SWCNT-TFT channel. Inset: schematic of back gate CNT-TFT device. (c) I-V characteristics of benzyl viologen-treated TFTs (5 mM). (d) G-band of Raman spectra at an excitation energy of 2.41 eV of the pristine SWCNTs (diamond) and that of the BV-doped SWCNTs (circle).

II-B. Adaptive Logic Circuits with Doping-Free Ambipolar Carbon Nanotube Transistors

Figure 3a shows a logic gate using four ambipolar TFTs. The NOR gate was realized when a *V*DD of 4 V was applied to the source of Tr1 and ground to the source of Tr2 and Tr4. In this case, Tr1 and Tr3 behave as p-type transistors and Tr2 and Tr4 behave as n-type transistors, following the above inverter principle. By combining *V*A and *V*B, a NOR function was obtained, as shown in Figure 3b. The adaptiveness of this logic gate was demonstrated by flipping *V*DD and ground, i.e., a VDD of 4 V

was applied to the source of Tr2 and Tr4 and ground to the source of Tr1. When the same bias combinations of VA and VB are applied, a NAND function was achieved. In this case, Tr1 and Tr3 behaved as n-type transistors and Tr2 and Tr4 behaved as p-type transistors, which is the opposite of the NOR gate. We emphasize that two functions of NOR and NAND gates were realized by using one set of logic gates.

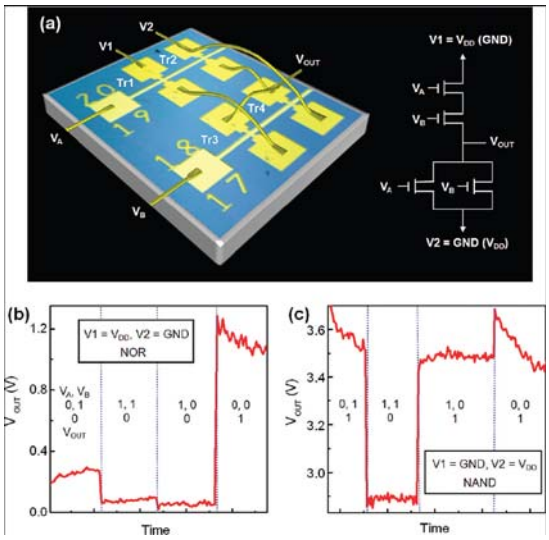

Figure 3. (a) Schematic view of adaptive logic gate (left) and circuit diagram (right). (b) Characteristics of NOR gate when V1) VDD and V2) GND, and (c) NAND gate when V1) GND and V2) VDD.

III. Significant Technical Progress at University of Pittsburgh and University of Texas at Dallas

III-A. Reduction-Controlled Viologen in Bisolvent as an Environmentally Stable n-Type Dopant for Carbon Nanotubes

The Poole – Frenkel emission (PF) model was utilized to explain temperature dependences of the I-V curves for both metallic and semiconducting CNT on the same samples. PF emission is governed by the relationship:

$$J \propto n_0 V \exp\left[-\frac{q}{kT}\left(\Phi_B - \sqrt{\frac{qV}{\pi d \varepsilon_s \varepsilon_0}}\right)\right] \quad (1)$$

where $J = I_{sd}$, n_0 the carrier density, V = V_{sd}, Φ_B is the trap barrier height, d is the length of the channel, and $\varepsilon_s\ \varepsilon_0$ the CNT dielectric constant and the vacuum permittivity, respectively.

Using this model, we first assume that the hopping states in the insulating region are away from the intrinsic Fermi level of the CNT. This assumption is reasonable, since if quantization in the length direction (onset from electron irradiation) occurs, there will be a discrete set of states (hopping states) located away from the Fermi level. As the Fermi level crosses through the insulator bandgap (via application of a back-gate voltage V_g) the barrier height modulation is determined by the energy difference between the gap states and the CNTs Fermi level. Any variation (metallic or semiconducting CNT) of the trap barrier height was found to have an exponential relationship with respect to applied V_g, a reflection of a barrier dependent on the energy difference between the trap state and the initial energy level.

However, the barrier height saturates at a minimum for metallic CNTs (Hf contacts for source/drain electrodes) and different phenomenon dominates. Theoretical calculations have indicated hopping lengths and conductivity are affected by the variability and magnitude of the DOS. Saturation is explained as a result of localization length differences in metallic and semiconducting tubes. As in a variable-range hopping model, an additional competing factor determined by the hopping distance and localization length can be added to the basic Poole Frenkel model. Equation (1) takes the form:

$$J \propto n_0 V \exp\left[-\frac{q}{kT}\left(\Phi_B - \sqrt{\frac{qV}{\pi d \varepsilon_s \varepsilon_0}}\right)\right] \cdot \exp[-\alpha] \qquad (2)$$

with $\alpha = \frac{2R}{\xi(V_{sd},T)}$, R = distance between hopping states, and $\xi(V_{sd},T)$ the localization length.[27] In metallic CNT, the electron irradiation generates a very small localization length and a decreased carrier wavefunction overlap that limits conductivity.

In contrast to the metallic case, semiconducting nanotubes (With Ti contacts) have a nonlinear quadratic energy dispersion relation near the valence and conduction band edges. The valence band and conduction band edges dominate conduction mechanism properties – dependent upon contact metal work function alignment and magnitude of V_g applied. The trap barrier height is determined via the difference between the valence band edge vHs and the final hopping state. As a result of near zero saturation barrier, semiconducting CNT must have a much larger localization length/shorter hopping distance due to the exponentially varying DOS with small α.

The exponential dependence of the traps on gate voltage for the semiconducting CNT is again synonymous with a trap barrier height dominated by the energy difference between the final hopping state and the initial state. If the previous results by Nosho *et al* are plotted on a logarithmic access, the same association for Schottky barrier height is observed. Although the nature of the barriers is quite different, the dominant factor is an energy difference between initial and final states, where Fermi level modulation varies the barrier height. In addition to the channel, the CNT contact region must contain traps/gap states. In the off-state, carriers tunneling through the contact – CNT interface due to the presence of gap states in this region can contribute to I_{sd}. We further observed that electron irradiated devices exhibit substantially higher off-state current (nA range) than non-irradiated devices. The inclusion of gap/trap states may decrease contact resistance by improving tunneling, but subsequently reduce the on/off ratios possible due to increased tunneling leakage current.

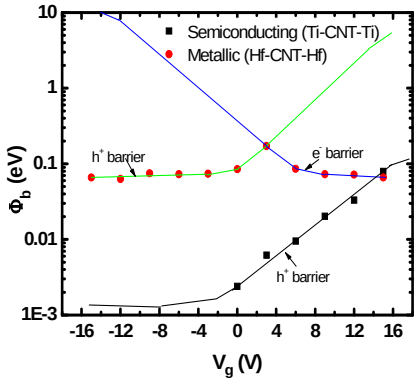

Figure 4. (a) Trap barrier heights for the Hf and Ti devices as a function of gate voltage. The Hf device barrier measurements can be split into contributions dependent on carrier type. The exponential barrier relationship is consistent with re-plotted results from Nosho *et al*.

IV. Publications

1. S. Y. Jeong et al. Chirality-specific transport phenomena of isolated singlewalled carbon nanotube, Phys. Stat. Sol. B 244, 4204 (2007).
2. Seung Yol Jeong, Seong Chu Lim, Dong Jae Bae, Young Hee Lee, Hyun Jin Shin, Seon-Mi Yoon, Jae Young Choi, Ok Hwan Cha, Mun Seok Jeong, David Perello, and Minhee Yun, "Photocurrent of CdSe nanocrystals on singlewalled carbon nanotube-field effect transistor", Appl. Phys. Lett., 92(24), 243103-1~3 (2008)
3. Seung Yol Jeong, Sang Hyun Jeon, Gang Hee Han, Kay Hyeok An, Dong Jae Bae, Seong Chu Lim, Ha Ryong Hwang, Chang Soo Han, and Young Hee Lee, 'Efficient Synthesis of Individual Single-

Walled Carbon Nanotube by Water-Based Catalyst with Poly(vinylpyrrolidone)', Journal of Nanoscience and nanotechnology, 8(1), 329-334, (2008)

4. David Perello et. al., “Schottky Barrier Engineering in Carbon Nanotube with Various Metal Electrodes”, Preoceedings of Nanotechnology 2007, 7th IEEE-NANO, Hong Kong
5. Innam Lee, Ho Il park, Seongyong Park, Moon J. Kim, and Minhee Yun, “Highly Reproducible Single Polymer Nanowires using Electrophoresis Method”, Nano, 3(2) 75-85 (2008)
6. Woo Jong Yu, Seung Yol Jeong, Ki Kang Kim, Bo Ram Kang, Dong Jae Bae, Min Baek Lee, Seung Hun Hong, Sunanda Prabhu Gaunkar, Didier Pribat, David Perello, Minhee Yun, Jae-Young Choi, and Young Hee Lee, ‘Bias-induced doping engineering with ionic adsorbates on singlewalled carbon nanotube thin film transistor’, New J. Phys. 10, 113013 (2008)
7. Soo Min Kim, Jin Ho Jang, Ki Kang Kim, Hyeon Ki Park, Jung Jun Bae, Woo Jong Yu, Il Ha Lee, Gunn Kim, Duong Dinh Loc, Un Jeong Kim, Eun-Hong Lee, Hyeon-Jin Shin, Jae-Young Choi, and Young Hee Lee, 'Reduction-Controlled Viologen in Bisolvent as an Environmentally Stable n-Type Dopant for Carbon Nanotubes', J. Am Chem. Soc., 131(1), 327-331 (2009)
8. Bo Ram Kang, Woo Jong Yu, Ki Kang Kim, Hyeon Ki Park, Soo Min Kim, Yongjin Park, Gunn Kim, Hyeon-Jin Shin, Un Jeong Kim, Eun-Hong Lee, Jae-Young Choi, and Young Hee Lee 'Restorable type conversion of carbon nanotube transistor using pyrolytically controlled antioxidizing photosynthesis coenzyme', Advanced Functional Materials.,19,2553-2559 (2009)
9. Woo Jong Yu, Un Jeong Kim, Bo Ram Kang, Il Ha Lee, Eun-Hong Lee and Young Hee Lee, 'Adaptive Logic Circuits with Doping-Free Ambipolar Carbon Nanotube Transistors', Nanoletters, 9(4), 1401-1405(2009)
10. Chandan Biswas, Ki Kang Kim, Hong-Zhang Geng, Hyeon Ki Park, Seong Chu Lim, Seung Jin Chae, Soo Min Kim, and Young Hee Lee, Michael Nayhouse and Mingee Yun 'Strategy for High Concentration Nanodispersion of Single-Walled Carbon Nanotybes with Diameter Selectivity', J. Phys. Chem. C., 113(23), 10044-10051(2009)
11. David J. Perello, Dong Jae Bae, Moon J. Kim, Dong Kyu Cha, Seung Yol Jeong, Bo Ram Kang, Woo Jong Yu, Young Hee Lee, and Minhee Yun, “Quantitative experimental analysis of Schottky barriers and Poole-Frenkel emission in carbon nanotube devices”, IEEE Transactions on Nanotechnology, 8(3), 355-360 (2009)

12. Woo Jong Yu, Bo Ram Kang, Yo-Sep Min and Young Hee Lee, 'Majority Carrier Type Conversion by Floating Gate in Carbon Nanotube Transistors', Adv. Mat., 21 (2009)
13. David J. Perello, Woo Jong Yu, Dong Jae Bae, Seung Jin Chae, M.J. Kim, Young Hee Lee, and Minhee Yun, 'Analysis of hopping conduction in semiconducting and metallic carbon nanotube devices', J. Appl. Phys., 105(12),124309-1~124309-5 (2009)
14. F. Gunes, G. H. Han, K. K. Kim, E. S. Kim, S. J. Chae, M. H. Park, H.-K. Jeong, S. C. Lim and Y. H. Lee 'Large Area Graphene-Based Flexiable Transparent Conducting Films', NANO, 4(2), 83-90 (2009)

V. Presentations

- Domestic

1. **K. K. Kim**. J. J. Bae, S. M. Kim, K. H. An, D. J. Bae, Young Hee Lee, ‘Modulation of Opticacal Properites of single-walled carbon nanotubes by $AuCl_3$’ , 2008 Spring meeting of Korean Physical Society, Apr. 17, 2008, Deajeon Convention Center, Korea, P.78
2. **J. H. Jang**, S. M. Kim, K. P. So, S. J. Chae, S. C. Lim, Young Hee Lee, 'Oxygen and Ar Ion Irradiations and In-siut I-V Characterizations of Carbon Nanotubes', 2008 Spring meeting of Korean Physical Society, Apr. 17, 2008, Deajeon Convention Center, Korea, P.106
3. **I. H. Lee**, G. H. Han, E. S. Kim, Young Hee Lee, 'Growth Behavior of Carbon Nanotubes Forest Dependent on the Pressure', 2008 Spring meeting of Korean Physical Society, Apr. 17, 2008, Deajeon Convention Center, Korea, P.163
4. **S. J. Chae**, J. H. Jang, I. H. Lee, Young Hee Lee, 'Growth of long singel-walled carbon nanotube(SWCNTs) arrays on a Si substrate using lamina flow', 2008 Spring meeting of Korean Physical Society, Apr. 17, 2008, Deajeon Convention Center, Korea, P.164
5. **S. M. Kim**, K. K. Kim, H. K. Park, J. J. Bae, Young Hee Lee, 'The separation of semiconducting SWCNTs from the matallic SWCNTs using P3HT', 2008 Spring meeting of Korean Physical Society, Apr. 17, 2008, Deajeon Convention Center, Korea, P.169
6. **B. R. Kang**, David Perello, Moon J. Kim, DongKyu Cha, G. H. Han, D. J. Bae, S. Y. Jeong, Y. H. Lee, Minhee Yun, 'Engineering of Schottky Barrier in Carbon Nanotues with several metal electrodes', The 14th International Symposium on the Physics of Semiconductors and Applications , Ramada plaza hotel, Jeju, August 28, 2008. Korea P.226

7. **W. J. Yu**, S. Y. Jeong, K. K. Kim, B. R. Kang, D. J. Bae, M. B. Lee, S. H. Hong, S. P. Gaunkar, D. Pribat, D. Perello, M. Yun, J. Y. Choi, and Y. H. Lee, 'Ionic adsorbates doping engineering by bias on singlewalled carbon nanotube thin film transistor', The 14th International Symposium on the Physics of Semiconductors and Applications , Ramada plaza hotel, Jeju, August 28, 2008. Korea P.225
8. **S. M. Kim**, H. J. Shin, K. K. Kim, S. M. Yoon, S. J. Kim, H. K. Park, J. Y. Choi, Y. H. Lee, 'Tailoring Electronic Structures of Carbon Nanotubes by Solvent with Electron Donating and Withdrawing Groups', 2008 Fall meeting of Korean Physical Society, Gwangju Convertion Center, Oct. 24, 2008. P.60
9. **S. J. Chae**, J. H. Jang, I. H. Lee, Y. H. Lee, 'Effect of Hydrogen Amount on cm-long Singlewalled Carbon Nanotube(SWCNTs) Arrays', 2008 Fall meeting of Korean Physical Society, Gwangju Convertion Center, Oct. 24, 2008. P. 100
10. **W. J. Yu**, S. Y. Jeong, K. K. Kim, B. R. Kang, D. J. Bae, M. B. Lee, S. H. Hong, Sunanda Prabhu Gaunkan, Didier Pribat, David Perello, M. H. Yun, J. Y. Choi, Y. H. Lee, 'Optimization of the Performance of Carbon Nanotube Transparent Conductin Films', 2008 Fall meeting of Korean Physical Society, Gwangju Convertion Center, Oct. 24, 2008. P. 161
11. **W. J. Yu**, S. Y. Jeong, K. K. Kim, B. R. Kang, D. J. Bae, M. B. Lee, S. H. Hong, Sunanda Prabhu Gaunkar, Didier Pribat, David Prerllo, M. H. Yun, J. Y. Choi, Y. H. Lee, 'Doping control of ionic adsorbates by induced-bias on carbon nanotube thin film transistor', 2nd Sungkyunkwan University-Hiroshima University Workdhop on Advanced Materials Research, Sungkyunkwan University, Nov. 9, 2008. P.50
12. **S. J. Chae**, J. H. Jang, I. H. Lee, Y. H. Lee, 'Lateral growth of long Single-Walled Carbon nanotube(SWCNTs) arrays on a Si substrate', 2nd Sungkyunkwan University-Hiroshima University Workdhop on Advanced Materials Research, Sungkyunkwan University, Nov. 9, 2008. P.58
13. **S. M. Kim**, 'Tailoring Electronic Structures of Carbon Nanotubes by Solvent with Electron Donating and Withdrawing Groups', 2nd Sungkyunkwan University-Hiroshima University Workdhop on Advanced Materials Research, Sungkyunkwan University, Nov. 9, 2008. P.61
14. **Il Ha Lee**, Jiwoon Im, Un Jeong Kim, Eun Ju Bae, Kyoung-Kook Kim, Eun Hong Lee, Seunghun Hong, Yo-Sep Min and Young Hee Lee1, 'Vertically Aligned Single-walled Carbon Nanotubes at Low Temperature', 5th Japan-Korea Symposium on Carbon Nanotube, Haeundae Grand Hotel, Nov. 10, 2008. P. 60

15. **Soo Min Kim**, Jin Ho Jang, Ki Kang Kim, Hyun Ki Park, Jung Jun Bae, Woo Jong Yu, Il Ha Lee, Gunn Kim, Duong Dinh Loc, Un Jeong Kim, Eun-Hong Lee, Hyeon-Jin Shin, Jae-Young Choi, and Young Hee Lee, 'Reduction-Controlled Viologen in Bisolvent as an Environmentally Stable n-Type Dopant for Carbon Nanotubes', 5th Japan-Korea Symposium on Carbon Nanotube, Haeundae Grand Hotel, Nov. 10, 2008. P. 71
16. **Woo Jong Yu**, Un Jeong Kim, Bo Ram Kang, Il Ha Lee, Eun-Hong Lee and Young Hee Lee, 'Adaptive Logic Circuits with Doping-Free Ambipolar Carbon Nanotube Transistors', 5th Japan-Korea Symposium on Carbon Nanotube, Haeundae Grand Hotel, Nov. 10, 2008. P. 100

- International

1. **W. J. Yu**, S. Y. Jeong, K. K. Kim, B. R. Kang, D. J. Bae, M. B. Lee, S. H. Hong, S. P. Gaunkar, D. Pribat, D. Perello, M. Yun, J. Y. Choi, and Y. H. Lee, 'Bias induced doping engineering with ionic adsorbates on singlewalled carbon nanotube thin film transistor', NT08, Le Corum, Montpellier, July 3, 2008. France, P.73
2. **I. H. Lee**, J.Im, U. J. Kim, G. H. Han, K. K. Kim, E. H. Lee, S. Hong, Y. S. Min, and Y. H. Lee, 'Vertical growth of single-walled carbon nanotubes using water PECVD', NT08, Le Corum, Montpellier, July 3, 2008. France, P.73
3. **Y. H. Lee**, 'Carbon Nanotubes Thin Film Transistors: CVD approach', ITC09, Ecole polytechnique, Franec, March 5-6, 2009.
4. **Y. H. Lee**, 'Doping Strategy of Carbon Nanotues', IWEPNM 2009, Kirchberg, Austria, March 12, 2009. P.137
5. **Soo Min Kim**, Jin Ho Jang, Ki Kang Kim, Hyeon Ki Park, Jung Jun Bae, Gunn Kim, Jae Young Choi, Young Hee Lee, 'Reduction-Controlled Viologen In Bisolvent as an Environmentally Stable n-Type Dopant for Carbon Nanotubes', IWEPNM 2009, Kirchberg, Austria, March 10,2009. P.94

VI. Future Plan

Over the previous years we have refined our approach of fabricating multiple electrodes and different metals to the point where over a hundred devices can now be easily fabricated on a single long CNT. All exposures of the CNTs will be performed with optical lithography, so as to avoid oxide charge trap generation or other perturbations to the CNT. Through the use of UV

exposure cleaning, avoidance of electron exposure, and improved characterization ability, we are in the process of characterizing devices with 4 metals per nanotube and 100 or more transistors per nanotube. Using such a setup, I-V and temperature measurements have been fit to the Schottky model, and regimes where image force lowering is significant and negligible are currently being identified. Furthermore, contact resistance as a function of metals on the same CNT has recently been observed with a very clear dependence on metal wet – ability and valence band structure. This data is preliminary at this time, and will be fully examined in the next half year. Preliminary results have also indicated that threshold voltage and existence of hysteresis are strongly a function of metal contact type and post-processing, and will be explored in depth over the next year as part of the CNT contact study. By combining all the efforts we have been doing so far, we are under process of fabricating Peltier device with nanotube network transistors using free standing SiN substrate.